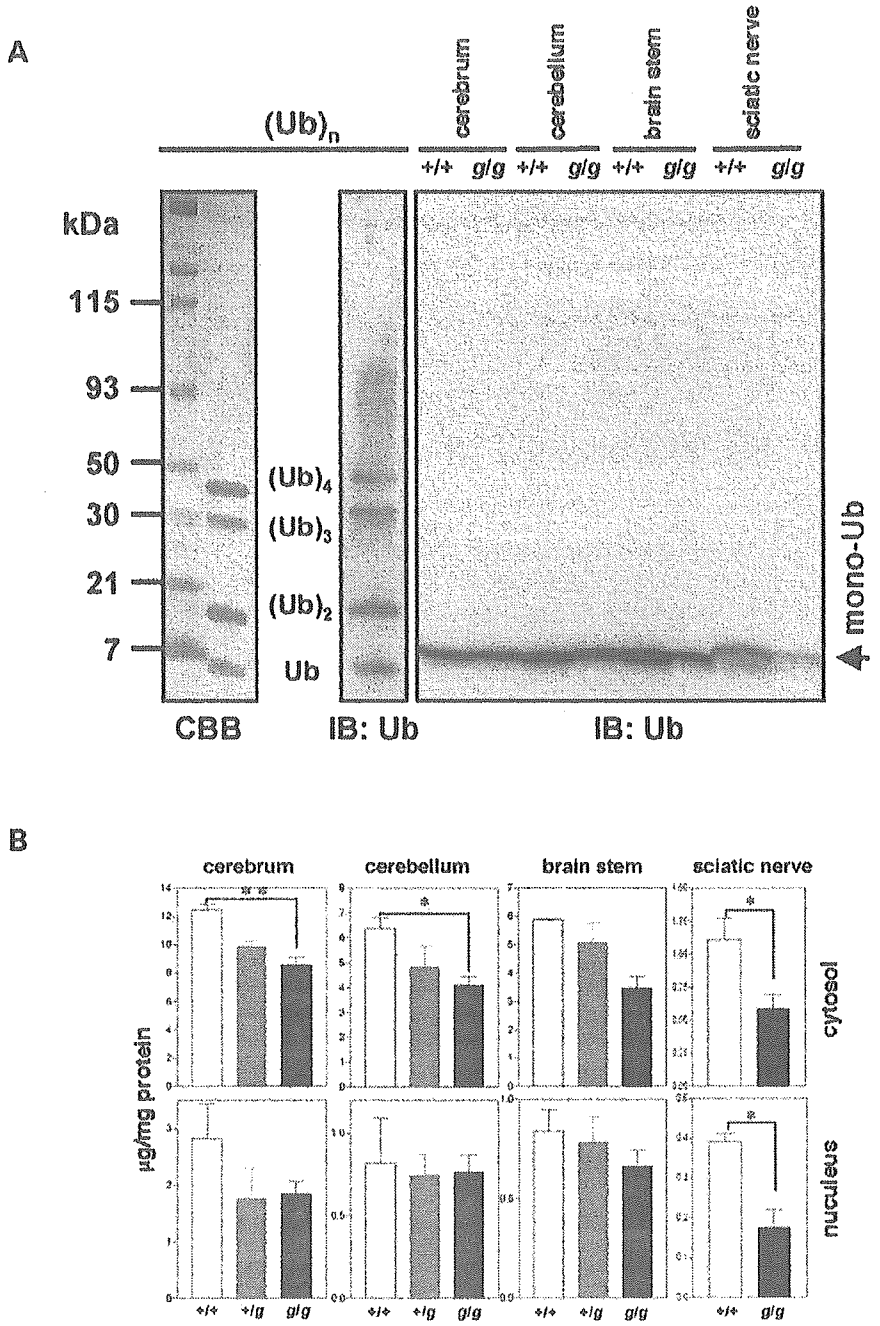

Figure 3. Loss of UCH L1 decreases the level of monoubiquitin. (**A**) A mixture of 1 μg ubiquitin and 4 μg poly-Ub was subjected to SDS–PAGE and stained with coomassie brilliant blue (left panel). Ten percent of this mixture was electrophoresed and immunoblotted with a monoclonal antibody to Ub (Chemicon) that recognizes both conjugated and unconjugated mono-/poly-Ub in denatured states (middle panel). Cytosolic fractions (20 μg) from various neuronal tissues of wild-type and *gad* mice were immunoblotted using the same antibody (right panel). (**B**) Levels of free mono-Ub in cytosolic (upper) and the nuclear (lower) fractions were measured by radioimmunoassay (16) in various brain structures from mice less than 2 weeks old ($n = 5$ for cerebrum, cerebellum and brain stem; $n = 4$ for sciatic nerve). Mean values with SEM are shown as open (+/+), gray (+/−) or black (*g/g*) bars. $^{**}P < 0.01$; $^{*}P < 0.05$.

adeno-*Uch l1* transfected cell to β-*gal*-transfected cell were 2.3 ± 0.2 to bands corresponding to mono-Ub and 1.5 ± 0.2 to bands corresponding to MW50-115; $n = 3$, corrected by β-actin).

Next, mice carrying a *Uch l1* transgene under control of the EF-1α promoter were generated (Fig. 5A). These mice exhibit no apparent neurological phenotype during life. However, transgenic (Tg) mouse expressing a high copy number of

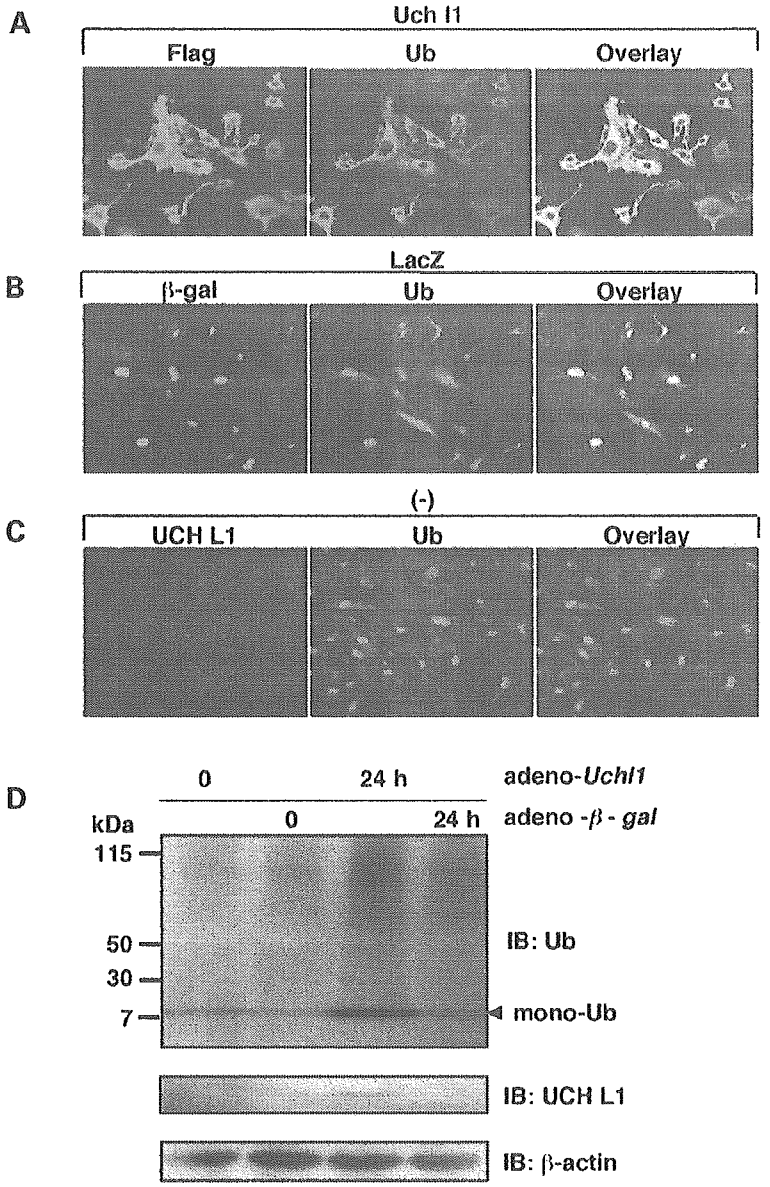

Figure 4. Overexpressed UCH L1 co-localizes with ubiquitin and increases ubiquitin levels in cultured cells. (A–C) E13.5 primary mouse embryonic fibroblasts (MEF) cells were transfected with adenovirus vectors expressing either *Uch l1* (A) or β-gal (B) or not transfected (C). UCH L1 was induced using Cre recombinase for 24 h. Antibodies to flag-tag and β-gal were used for immunostaining to exogenic UCH L1 and β-gal (A, B; left panels). An absence of immunoreactivity to anti-UCH L1 showed the lack of endogenous UCH L1 expression in MEF cells (C; left panel). MEF cells were also labeled with polyclonal anti-Ub (Sigma; A–C; middle panels). Immunoreactivities to anti-Ub/-UCH L1 completely merge in MEF cells transfected with adeno-*Uch l1* (A; right panel), but not in cells transfected with β-gal (B; right panel) and not transfected (C; right panel). Ub localization appears to be recruited to the UCH L1. (**D**) Cell lysates were immunoblotted with anti-Ub (Chemicon) or anti-UCH L1 at the indicated times (upper and middle panels). The same membrane was re-blotted with an antibody to β-actin (lower panel). Band intensities were measured at the bands corresponding to mono-Ub and poly-ubiquitinated bands at MW50-115 kDa and normalized by β-actin intensities.

foreign DNA and high-level of mRNA from *Uch l1* transgene were all infertile ($n = 6$, manuscript in preparation). Therefore, we examined two of these infertile Tg mice, 11 and 22 (Fig. 5B). Immunohistochemistry of brain sections showed increased levels of UCH L1 immunoreactivity in the nervous system of Tg mice (Fig. 5C; left panel, cerebral cortex; right panel, cerebellum). The antibody to Ub that preferentially stains free mono-Ub showed a significant increase in Ub immunoreactivity in Tg mice (Fig. 5D; cerebellum). Immunoblotting also showed the increased level of mono-Ub in Tg mice (Fig. 5E; band intensity for mono-Ub of Tg 22 to wild-type was 2.3 in cerebrum and 1.5 in cerebellum). These data show that UCH L1 overexpression increases the level of mono-Ub in the cultured cells and nervous system *in vivo*.

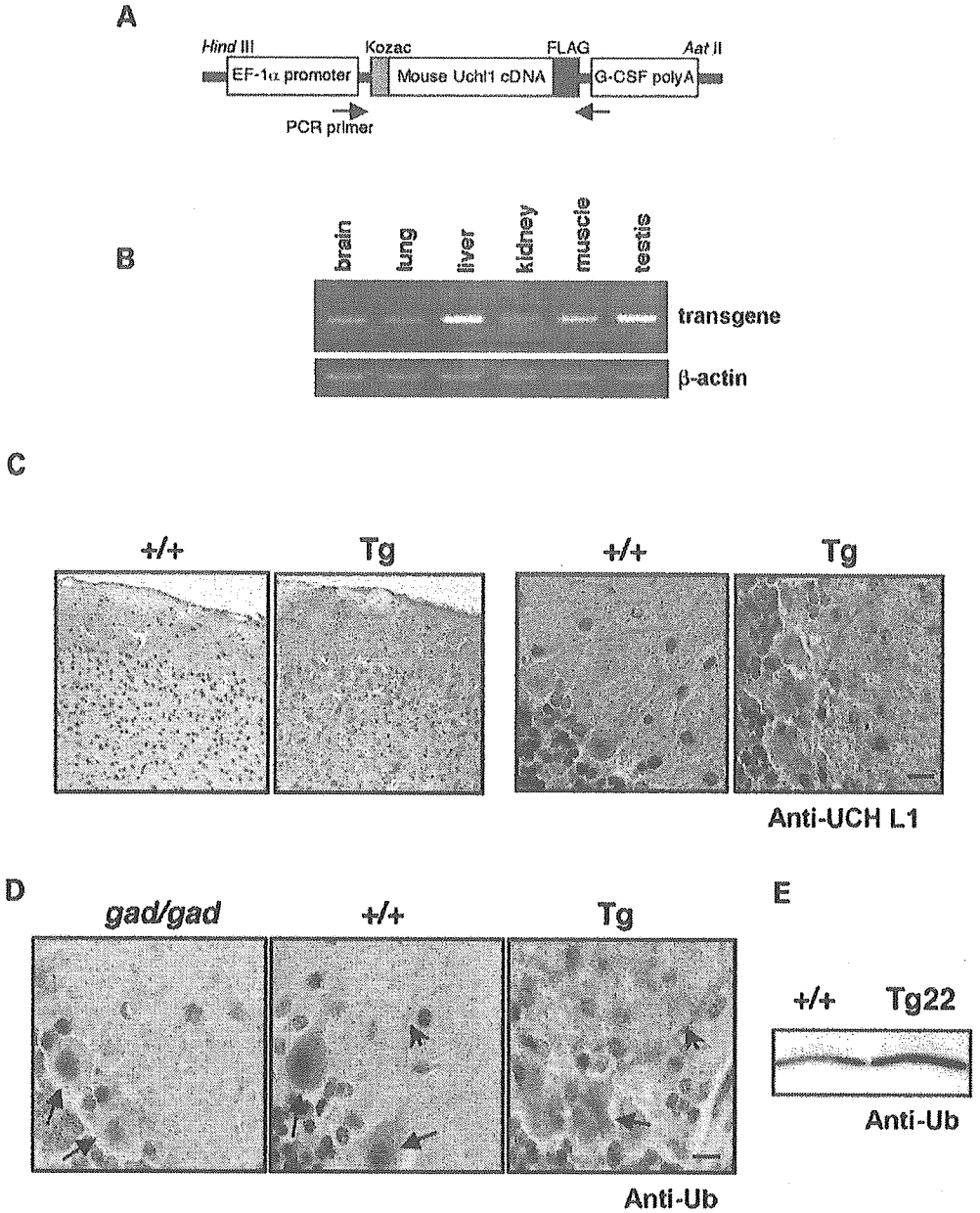

Figure 5. UCH L1 overexpression increases ubiquitin level in the mouse nervous system. (**A**) Construction of the transgenic vector. Flag-tagged mouse *Uch l1* cDNA was subcloned into pEF-Bos vector that carries EF-1α promoter. (**B**) Total RNAs of 5 μg from various organs of transgenic (Tg) mouse 22 were subjected to RT–PCR using specific primers to transgenic *Uch l1* cDNA (upper panel) and β-actin (lower panel). (**C**) Immunohistochemisty to anti-UCH L1 antibody to cerebral cortex (left panels) and cerebellum (right panels) from Tg 22 and wild-type mouse. Scale bars, 20 μm. (**D**) Cerebellar sections from *gad* (*gad/gad*), wild-type (+/+), and UCH L1 transgenic mice (Tg 22) brains were analyzed by immunohistochemistry using polyclonal anti-Ub (Sigma) as the primary antibody. Ub reactivity was increased in Tg 22 mouse. The *gad* mouse showed decreased immunoreactivity to anti-Ub. Arrows and arrowheads indicate Purkinje cell body and neurites, respectively. Scale bars, 20 μm. Twenty micrograms of proteins of the cerebrum (**E**) and cerebellum from Tg 22 and wild-type mouse were subjected to SDS–PAGE and immunoblotted with anti-Ub.

Mechanism by which UCH L1 increases Ub levels

The basis of the UCH L1-mediated increase in Ub levels was examined using three different approaches. First, Ub transcriptional regulation was examined in both wild-type and *gad* mice. The mRNA levels of all four Ub genes, *Uba52*, *s27a*, *UbB* and *UbC*, were analyzed by quantitative PCR but no significant differences were observed between wild-type and *gad* mice (Fig. 6A). A reporter assay using the *UbC* gene promoter also showed no effect of UCH L1 on

transcriptional activation of the *UbC* gene (Fig. 6B). These experiments showed that UCH L1 does not upregulate Ub levels via transcriptional activation.

Second, to address the possibility that a reduction in the release of mono-Ub from poly-Ub or Ub-conjugated proteins affects the level of free mono-Ub in *gad* mice, UCH L1-catalyzed release of mono-Ub from substrates was tested. UCHs can generate mono-Ub from poly-Ub and peptide–ubiquityl amides *in vitro* (12). However, no enhanced intensity corresponding to the release of Ub from poly-Ub (Fig. 3A; compare left and right panels) or mass spectra corresponding to the hydrolysis of peptide–ubiquityl amides (Fig. 1E) was observed in the *gad* mouse immunoprecipitates from brain lysates. Alternatively, an unknown substrate could be upregulated as poly-Ub-conjugated proteins (multi-Ub) in *gad* mice. Therefore, multi-Ub levels were measured in soluble mouse brain lysates by sandwich ELISA using antibody FK2 that is specific for multi-Ub (16–18) (Fig. 6C). No difference in the level of multi-Ub was observed between the wild-type and the *gad* mouse at less than 2 weeks of age. These data argue against the hypothesis that the deficiency in UCH L1-catalyzed release of mono-Ub from multi-Ub is responsible for the decreased level of Ub observed in the *gad* mouse.

Third, the effect of UCH L1 expression on Ub metabolism was examined in MEF cells transfected with either adeno-*Uch l1* or -β-*gal*. Mono-Ub levels were monitored for 30 h after pulse-chase labeling and Ub degradation was compared by autoradiography. Ub half-life was extended in MEF cells transfected with UCH L1 (Fig. 6D). Since lysosomes are implicated as the site of Ub degradation, we examined the effect of the lysosomal inhibitor EST (2,3-*trans*-epoxysuccinyl-L-leucylamide-3-methyl butane ethyl ester) on Ub metabolism (19,20). EST extended Ub half-life in both adeno-*Uch l1*- and adeno-β-*gal*-transfected MEF cells (Fig. 6D) and, under these conditions, mono-Ub degradation was comparable between the adeno-*Uch l1*-transfected cells and the control cells (Fig. 6D).

These data suggest that UCH L1 affects Ub degradation and alters its metabolism, and that Ub degradation occurs in lysosomes.

UCH L1 affinity for Ub appears to be indispensable for the maintenance of Ub levels

To further clarify the effect of UCH L1 on Ub levels, his-tagged *Uch l1* and mutants were transfected into dopamine-producing SH-SY5Y neuronal cells (Fig. 7). UCH L1 and Ub were then visualized using confocal immunofluorescence microscopy. Cells transfected with wild-type *Uch l1* showed a relative increase in Ub immunoreactivity compared with mock-transfected cells (anti-Ub; Sigma, polyclonal; Fig. 7A and E) consistent with Ub upregulation by UCH L1. *Uch l1*^{I93M}, implicated in the pathogenesis of PD, also increased Ub immunoreactivity comparable to wild-type *Uch l1* (Fig. 7B and E). Increased Ub immunoreactivity was also evident in cells transfected with *Uch l1*^{C90S}, which retains Ub binding affinity but lacks C-terminal hydrolase activity (Fig. 7C and E; Table 1) (9). However, significant increase in Ub immunoreactivity was not observed with mutant *Uch l1*^{D30K} (Fig. 7D and E), which carries a charge reversal on the surface of the protein that is presumed to interact with cationic residue of Ub (21). This mutant protein exhibits markedly lower affinity for Ub and has no hydrolase activity (Table 1). These data suggest that UCH L1-mediated increases in Ub levels are a function of UCH L1 affinity for Ub rather than hydrolase activity.

DISCUSSION

In spite of the abundance of UCH L1 in the nervous system and its importance in the neurodegenerative diseases, the *in vivo* functions of UCH L1 have been remained unknown (6–13). The *gad* mouse and the UCH L1 transgenic mouse revealed a novel role for UCH L1 in neurons. Our data indicate that UCH L1 is associated with mono-Ub and elevates the level of mono-Ub in neuron. Previously, Doa4, a deubiquitinating enzyme belonging to UBPs, was reported to elevate the level of Ub in yeast, although the association of Doa4 with Ub was not mentioned (19). From a genetic complementation study, Doa4 was inferred to be involved in endosomal–lysosomal pathway (20). Our pulse-chase labeling using MEF cells suggests that UCH L1 affects Ub metabolism and extends its half-life by inhibiting Ub degradation. As an inhibitor of lysosomal function extended Ub half-life and partially diminished the effect of UCH L1, UCH L1 probably prevents Ub degradation in lysosomes. Thus, our results also suggest the link of DUBs to the endosome–lysomal pathway. Recently, it was demonstrated that Ub itself contains all the necessary signals for both targeting and degradation of monoubiquitylated proteins in the endosomal–lysosomal pathway, with the crucial Ub residues being Gln2, Phe4, Lys6, Leu8, Val26, Leu43, Ile44, Glu64 and Val70 (22,23). Possibly some fraction of free Ub itself is shunted into the endosome–lysosomal pathway and UCH L1 binding to Ub may suppress this route by masking Ub residues that are requisite for targeting. Alternatively, it may be possible that UCH L1 deubiquitylates ubiquitylated proteins before degradation within the endosome–lysosome pathway. However, UCH L1^{C90S}, lacking hydrolase activity, still retains the ability to maintain Ub levels, suggesting that physical association with UCH L1 rather than its deubiquitylating activity promotes Ub stability. Although UCH L1 can very slowly cleave poly-Ub and Ub-small molecule adducts *in vitro* (4), we did not find accumulation of such Ub species in *gad* mice. This finding may reflect functional redundancy between UCHs and UBPs. Alternatively, such Ub species may be detergent insoluble and exist within aggregates of Ub in dot-like structures observed in *gad* mice (10).

It has been long known that Ub-containing protein aggregates as hallmarks of various neurodegenerative conditions (2). Such aggregates are remnants of inadequate proteolysis and suggest either surpluses of aggregation-prone abnormal proteins or insufficiencies in Ub-dependent proteolysis (Fig. 8). PD caused by A53T and A30P mutations of α-synuclein appear to be the examples for the former case. These mutant proteins are more stable than wild-type and presumed to surpass the critical concentration of α-synuclein for oligomerization (24,25). The latter case appears to account for both a *Uch l1* gene deletion in the *gad* mouse and the parkin gene mutations in the patients with PD. Loss of function mutations in Parkin E3 ligase may prevent this enzyme from properly ubiquitylating putative

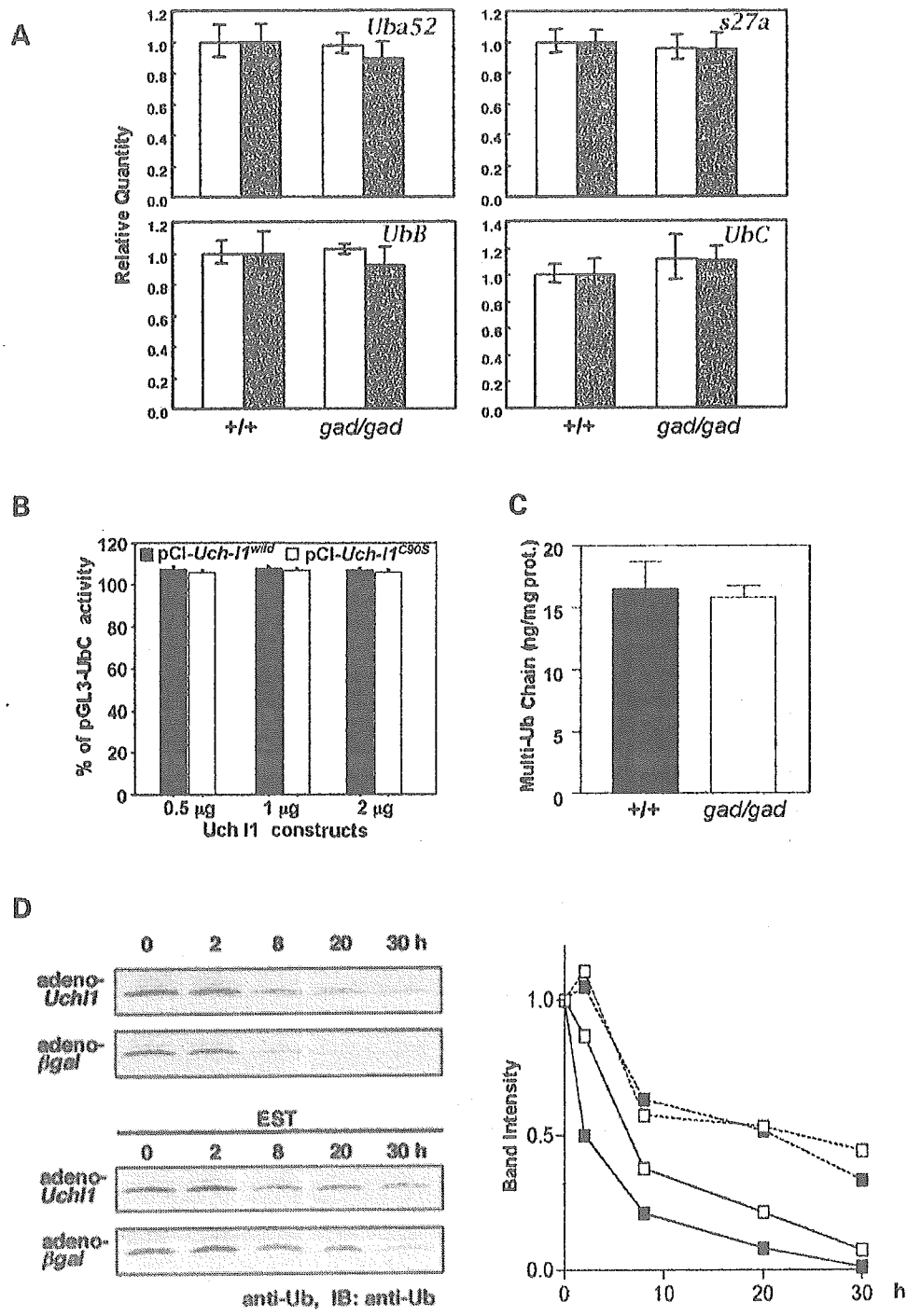

Figure 6. Effects of UCH L1 on transcription, processing and post-translational state of ubiquitin. (**A**) Quantitative RT–PCR for *Uba52*, *s27a*, *UbB* and *UbC* was performed using total RNA from wild-type and *gad* (*gad/gad*) cerebrum ($n = 3$). Mean values are shown with SEM. β-Actin (open bar) or GAPDH (solid bar) were used as internal controls. (**B**) Dual luciferase assay of a vector containing the +18 to +1227 bp region of the human Ub C promoter (pGL3-*UbC*) co-transfected with either UCH L1 (pCI-neo-*Uchl1*^{WT}; solid bar) or an active site mutant of UCH L1 (pCI-neo-*Uchl1*^{C90S}; open bar). Mean values from eight independent experiments are shown with SEM. (**C**) Levels of multi-Ub chain (conjugated poly-Ub) in cerebellum cytosolic fractions were measured by ELISA from 2-week-old mice ($n = 6$) (16–18). Mean values with SEM are shown as filled (+/+) or open (*gad/gad*) bars. (**D**) Adeno-*Uchl1*-transfected or adeno-β-*gal*-transfected MEF cells were labeled with [^{35}S]-Met. Autoradiograms of anti-Ub immunoprecipitates pulse-chased at the indicated times in the absence (left upper panels) or presence of EST (2,3-*trans*-epoxysuccinyl-L-leucylamide-3-methyl butane ethyl ester; left lower panels) are shown. Relative band intensities are quantified and mean values of two independent experiments are shown (right).

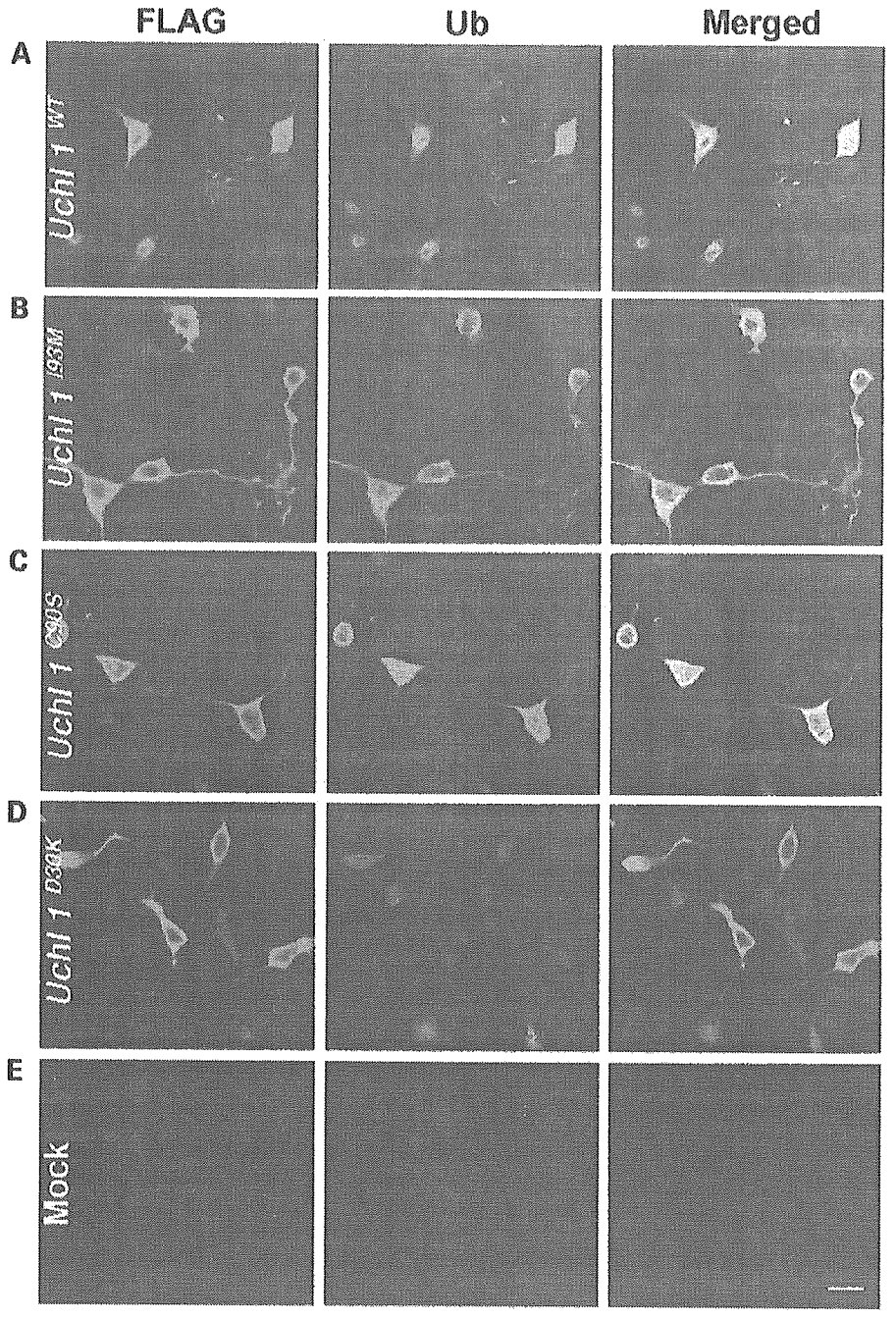

Figure 7. Effect of UCH L1 mutants on ubiquitin expression. Plasmids pcDNA3-*Uchl1*^{WT} (**A**), -*Uchl1*^{193M} (**B**), -*Uchl1*^{C90S} (**C**), -*Uchl1*^{D30K} (**D**) and vector alone (**E**) were transfected into SH-SY5Y cells and expressed. Antibodies against flag-tag and Ub (Sigma, polyclonal) were used to detect transfected UCH and endogenous Ub, respectively. The faint green staining (left panels) reflects non-specific staining of cells that escaped transfection. Scale bars, 20 μm.

substrates (26,27), causing substrate accumulation and toxicity to neurons at the substantia nigra. Loss of functional UCH L1 could also lead to inadequate ubiquitylation via decrease of free Ub. An initial pathological lesion begins at the synapse of the sciatic nerve in the *gad* mouse. Ub is known to be transported over long distances via slow axonal transport to synapse (28). Ub decrease and the consequent inadequate ubiquitylation of proteins may trigger increased levels of proteins that should undergo Ub-dependent degradation, resulting in the accumulation of such proteins within spheroids observed in *gad* mice (11). The *gad* mouse phenotypes resemble those of Charcot–Marie–Tooth diseases (CMT) in humans. Although there are no

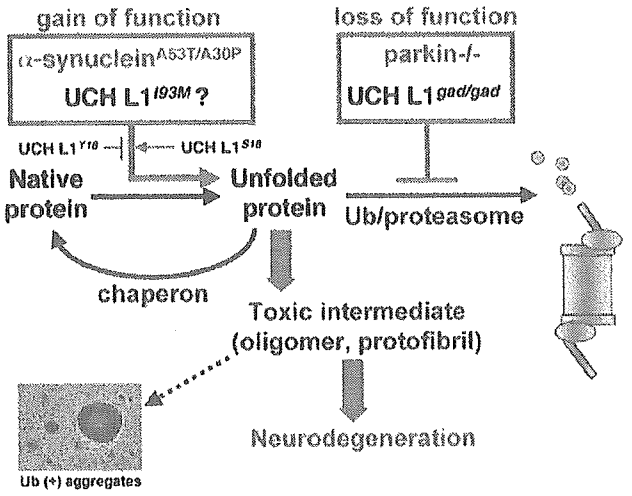

Figure 8. Common pathway of neurodegeneration. Unfolded proteins are refolded by molecular chaperons or degraded by the ubiquitin/proteasome pathway. The red boxes illustrate that excessive production of insoluble proteins by genetic defect (such as A53T/A30P mutations of α-synuclein in Parkinson's disease) or insufficiencies in the ubiquitin/proteasome pathway (such as *Uch l1* gene deletion in the *gad* mouse and the parkin gene mutations in the patients with PD) alter the proportion of denatured proteins within the cell. The accumulation of a toxic intermediate (oligomer or protofibril) is proposed to precede and promote neurodegeneration.

CMT or peripheral neuropathies that map to the proximity of the human *UCH L1* locus so far, immunohistological profiling of UCH L1 and Ub in peripheral nerves would be helpful in delineating a human *gad* analog.

Human *UCH L1* deletion mutants have not been reported although polymorphism and missense mutations of UCH genes are linked to PD (29–32). In idiopathic PD, particularly of Japanese or Chinese origin, UCH L1 gene polymorphism at position 18 is linked to a disease susceptibility (29–32). The S18Y mutation is common in Japanese and Chinese compared with Europeans and is reportedly protective for PD (19–32). Recently, UCH L1 was found to exhibit dimerization-dependent ubiquityl ligase activity at Lys63 of acceptor Ub molecules *in vitro* (13). Polyubiquitylated proteins linked to Lys48 of Ub are destined for proteasomal degradation, while those linked to Lys63 of Ub are stable. The protective variant Y18-UCH L1 exhibits diminished dimerization and ligase activities relative to S18-UCH L1, and therefore Y18-UCH L1 is predicted to accelerate degradation of proteins such as α-synuclein by making less stable species conjugated to Lys 63 of Ub. Thus, the decreased susceptibility to PD in individuals carrying the S18Y mutation could be explained by the low concentration of α-synuclein, which is yet confirmed *in vivo* (13) (Fig. 8). The I93M mutation in UCH L1 is reported in familial PD with dominant inheritance (9). α-Synuclein (dominant form) or the of parkin or DJ-1 (recessive forms) may also cause familial PD (33–35). The glycosylated form of α-synuclein is a substrate for parkin (36). Our present data indicate that UCH L1 upregulates Ub levels *in vivo*, and therefore UCH L1, parkin and α-synuclein appear to be interrelated with respect to Ub and ubiquitylation pathways. As with α-synuclein, the loss of UCH L1 function does not appear to cause PD (11,37). In patients carrying the UCH L1 mutation I93M, both ligase and hydrolase activities are presumed to be partially reduced (9,13). Our data show that UCH $L1^{I93M}$ enhances Ub immunoreactivity similar to UCH $L1^{WT}$ in transfected cells. Moreover, we did not find evidence for nigrostriatal dopaminergic pathology in either *gad* mouse heterozygotes or homozygotes. Therefore, an as yet unknown 'gain of toxic function' condition may underlie PD in patients carrying UCH $L1^{I93M}$ (Fig. 8).

Our results reveal that the fundamental defects in the *gad* mouse are due to a lack of UCH L1 and consequent Ub decrease. Ub and Ub-dependent proteolysis are involved in nearly all cellular processes and therefore it is likely that *gad* mice exhibit a wide variety of neuronal malfunctions that are not recognized by routine histology. Thus, in light of our present data we are currently re-evaluating *gad* mouse phenotypes including behavior, neuronal regeneration and apoptosis. These studies will broaden our understanding of the role of Ub pathways in neuronal function and neurodegenerative disorders.

MATERIALS AND METHODS

Plasmid and protein purification

Sequences encoding UCH L1 were amplified from a mouse brain cDNA library by polymerase chain reaction (PCR), and subcloned into either pQE-30 (Qiagen, Valencia, CA, USA) or pcDNA3 (Invitrogen, Groningen, The Netherlands) for expression in *E. coli* (for protein purification) or mammalian cells (for transfection), respectively. cDNA encoding UCH $L1^{gad}$ was obtained from a *gad* mouse brain by PCR. Another UCH L1 mutations were introduced by PCR-based site-directed mutagenesis (QuickChange Site-Directed Mutagenesis Kit, Stratagene, La Jolla, CA, USA) of template plasmids using primers designed to introduce specific mutations (D30K, C90S, I93M). Proteins overexpressed in *E. coli* were purified using Ni-agarose (Qiagen) as per the manufacturer's protocol and purified further by gel filtration using a Hi Load™ 16/60 Superdex 75 column (Amersham Pharmacia, Uppsala, Sweden).

Generation of adeno-vectors, antibodies and Ub level determination

Recombinant plasmids containing adeno-*Uch l1* and -β-*gal* were constructed using the Adenovirus Expression Vector Kit as per the manufacturer's instructions (Takara, Tokushima, Japan). Briefly, *Uch l1-flag* and β-*gal-flag* genes were inserted individually into the cosmid vector pAxCANLw containing the CAG promoter, the stuffer sequence and two loxP sequences. These recombinant cosmids were co-transfected into HEK 293 cells with a restriction enzyme-digested adenovirus DNA-TPC to generate a recombinant adenovirus through homologous recombination. Expression of the *Uch l1-* or β-*gal*-gene is achieved by removal of the stuffer sequence between the loxP sequences by Cre recombinase (expressed by co-transfection with pAx CANCre DNA).

Immunizing with different ubiquitin-carrier conjugates produced five antibodies and, among them, US-1 was found to be specifically reactive to mono-Ub (16). Immune complexes of US-1 and ^{125}I-mono-Ub were obtained by centrifuge and counted in a gamma counter. The inhibition for the tracer bound to the antibody in the presence of lysates was measured and mono-Ub level was determined from the standard curve generated by unlabeled Ub (16). Monoclonal antibody FK2 that recognizes conjugated-multi-ubiquitin chain was used for immunoassay (sandwich ELISA) for multi-ubiquitin chains as described (17,18). This ELISA system shows an only negligible reactivity to free-Ub (17).

Fractionation, immunoaffinity purification and immunoblotting

Mouse brains were homogenized in lysis buffer (50 mM NaH_2PO_4/300 mM NaCl/10 mM imidazole, containing a complete protease inhibitor cocktail, pH 8.0) and centrifuged at 70 000*g* for 1 h to yield a cytosolic fraction. The nuclear fraction was extracted with lysis buffer containing 10% NP-40 and 400 mM NaCl. Insoluble materials were dissolved with 8 M urea. For pull-down assays, 200 μg of His_6-tagged UCH $L1^{WT, C90S, D30K}$ and 40 μl of Ni-NTA Agarose (Qiagen) were added to 750 μl mouse brain lysate containing 6 mg total protein. After gentle rotation overnight at 4°C, the Ni-NTA beads were washed three times with 200 μl of wash buffer (50 mM NaH_2PO_4/300 mM NaCl/20 mM imidazole, pH 8.0). The beads were eluted with 3 × 40 μl elution buffer (50 mM NaH_2PO_4/300 mM NaCl/250 mM imidazole, pH 8.0) and subjected to SDS–PAGE, stained with Coomassie brilliant blue (CBB) or immunoblotted. Densitiometric analysises were done using software PD QUEST (BioRad). For TOF analysis, 1 μl samples were spotted onto H4 hydrophobic-coated Protein Chip Array (Ciphergen Biosystems, Palo Alto, CA, USA) after desalting with a C_{18} zip tip column. The ionized proteins were detected and accurate mass was determined based on TOF analysis. TOF mass spectra were collected in the positive ion mode and signal averages of 50 laser shots were used to generate each spectrum. After SDS–PAGE on a 10–20% gradient gel, protein bands migrating at ~8 kDa were excised and digested within the gel with trypsin (Sigma). Digested peptide samples were then introduced via nano-spray into a QSTAR Pulsar LC/MS/MS system (Applied Biosystems, Foster City, CA, USA). Immunoblotting was performed as described (10) using antibodies to Ub (1 : 100, Chemicon, MAB1510) and UCH L1 (1 : 1000, Chemicon, polyclonal). The Ub antibody MAB1510 is reactive to both free and conjugated forms of Ub in immunoblotting (15). The epitopes of UCH L1 antibody were confirmed to recognize the region encoded by other than exons 7 and 8 of *Uch l1* gene, by using UCH $L1^{gad}$ protein produced by *E. coli* expression system. Ub and $(Ub)_n$ were purchased from Boston Biochem, MA, USA.

Immunohistochemistry, immunofluorescence and electron microscopy

Twelve-week-old mouse brain and sciatic nerve sections were analyzed by immunocytochemistry as previously described (10) using antibodies to Ub that is predominantly reactive to free Ub in immuno-histochemistry (1 : 100, Sigma) and UCH-L1 (1 : 40, Medac; monoclonal). Antibodies to neurofilament-M (NF; 1 : 200, Chemicon, monoclonal), glial fibrillary acidic protein (GFAP; 1 : 200, Chemicon, monoclonal), proteolipid protein (PLP; 1 : 200, Chemicon, monoclonal) and myelin basic protein (MBP; 1 : 200, QED bioscience, monoclonal) were used as neuronal, astrocytes, oligodendrocytes, schwann cell markers, individually. For immunofluorescence studies, anti-mouse-Cy3 or -FITC or anti-rabbit-conjugated-Cy3 or -FITC (1 : 500, Jackson Immuno Research) were used as secondary antibodies. MEF cells and SH-SY5Y cells were analyzed by immunofluorescence using either anti-flag tag (1 : 200, Sigma) or anti-Ub (1 : 100, Sigma) as the primary antibodies. Ultrastrucal studies by electron microscopy were performed as described using sciatic nerve (11).

Quantitative RT–PCR analysis and dual luciferase assays

Primers for the mouse *Uch l3* and four ubiquitin genes were designed and comparative reverse transcription–PCR (RT–PCR) was performed using Taq Man probe with the ABI PRISM 7700 (Applied Biosystems) using total RNA from wild-type and *gad* mouse brain ($n = 3$). The dual luciferase assay was performed using the +18 to +1227 bp region of the human Ub C promoter generated from human genomic DNA as per the manufacturer's instructions (Promega).

Pulse chase analysis

Transfected MEF cells were washed and incubated with methionine-free medium for 1 h. The cells were then pulsed with 200 μCi/ml [^{35}S]-Met (NEN) for 1 h and then washed and chased with 30 mM methionine for 30 h. At 0, 2, 8, 20 and 30 h the cells were harvested for immunoprecipitation with anti-Ub. Following SDS–PAGE on a 15% gel, radioactive bands were detected using the image analysis software PD QUEST (BioRad).

Transgenic UCH L1 mouse

Flag tagged mouse UCH L1 was subcloned into pEF-Bos vector under the strong promoter EF-1α. This plasmid was linearized by digestion with *Hind*III/*Aat*II, gel-purified and extracted twice with phenol/chloroform. A 2 μg/ml solution of linearized plasmid was used for pronuclear microinjection. Offspring were screened for the presence of the transgene by PCR of tail DNA. Expression of transgenic *Uch l1* mRNA was confirmed by reverse transcription of total RNA (5 μg) and subsequent PCR using specific primers (Fig. 5A). Primers to β-actin were used for internal controls.

Molecular simulation

Mouse UCH L1 was automatically modeled using Modeler software with Insight (MSI) interface. Briefly, mouse UCH L1 was modeled after the data from the crystal structure of human UCH L3 using the ClustralW algorithm. Human UCH L3 was used to derive spatial restraints expressed as probability density functions (14). These functions are used to constrain C^{α}–C^{α} distances, main chain N–O distances, main chain and side chain dihedral angles, etc. The individual constraints were assembled

into a single molecular probability density function (MPDF). The three-dimensional protein model was then obtained by optimizing this MPDF. The optimization procedure itself employed a variable target function method with a conjugate gradient minimization scheme followed by an optional restrained simulated annealing molecular dynamics scheme.

Steady-state kinetics

Steady-state kinetic measurements were conducted at 25°C in assay buffer (50 mM HEPES pH 7.5, 0.5 mM EDTA, containing 0.1 mg/ml ovalbumin and 1 mM DTT). Concentrations of enzymes were 5 nM for UCH L1 and 5 mM for D30K- and C90S-UCH L1 mutants. Ubiquitin-7-amido-4-methylcoumarin (Ub-AMC; Boston Biochem, MA, USA) served as substrate at different concentrations, and AMC production was monitored continuously by fluorescence (Wallace 1420 multilabel counter, Perkin Elmer, Turk, Finland; $\lambda_{ex} = 355$ nm, $\lambda_{em} = 460$ nm). For competition/inhibition by ubiquitin, enzymes were pre-incubated with ubiquitin for 5 min at 25°C before adding substrates. Initial velocity data were used to determine values for K_m, K_i and k_{cat} from non-linear fits of the Michaelis–Menten equation with the program PRISM (GraphPad, San Diego, CA, USA).

ACKNOWLEDGEMENTS

We thank the following people for their contributions to this work: T. Kikuchi, T. Kokubo, R. Takahashi and Y. Imai for helpful discussions; S.-M. Tilghman for kind gift of *Uch l3*$^{\Delta 3\text{-}7}$ mouse; T. Kikuchi for technical assistance with tissue sections; A. Kanou for modeling (Ryoka Systems Inc.); K. Arimoto and J. Ando for TOF MASS analysis (Applied Biosystems); F. Melandri (Boston Biochem) for advice regarding steady-state kinetic measurements; S. Kohsaka for providing SH-SY5Y cells; and M. Shikama for the care and breeding of animals. This work was supported by grants-in-aid from the Ministry of Health, Labor and Welfare of Japan, grants-in-aid for scientific research from the Ministry of Education, Culture, Sports, Science and Technology of Japan, a grant from the Organization for Pharmaceutical Safety and Research, and a grant from Japan Science and Technology Cooperation. S.A. is a fellow of the Japan Society for the Promotion of Science (JSPS). Y.-L.W. is a fellow of the Japan Foundation for Aging and Health.

REFERENCES

1. Weissman, A.M. (2001) Themes and variations on ubiquitylation. *Nat. Rev. Mol. Cell. Biol.*, **2**, 169–178.
2. Tran, P.B. and Miller, R.J. (1999) Aggregates in neurodegenerative disease: crowds and power? *Trends Neurosci.*, **22**, 194–197.
3. Wilkinson, K.D., Laleli-Sahin, E., Urbauer, J., Larsen, C.N., Shih, G.H., Haas, A.L., Walsh, S.T. and Wand, A.J. (1999) The binding site for UCH-L3 on ubiquitin: mutagenesis and NMR studies on the complex between ubiquitin and UCH-L3. *J. Mol. Biol.*, **291**, 1067–1077.
4. Larsen, C.N., Krantz, B.A. and Wilkinson, K.D. (1998) Substrate specificity of deubiquitinating enzymes: ubiquitin C-terminal hydrolases. *Biochemistry*, **37**, 3358–3368.
5. Finley, D., Bartel, B. and Varshavsky, A. (1989) The tails of ubiquitin precursors are ribosomal proteins whose fusion to ubiquitin facilitates ribosome biogenesis. *Nature*, **338**, 394–401.
6. Wilkinson, K.D., Lee, K.M., Deshpande, S., Duerksen-Hughes, P., Boss, J.M. and Pohl, J. (1989) The neuron-specific protein PGP 9.5 is a ubiquitin carboxyl-terminal hydrolase. *Science*, **246**, 670–673.
7. Wilkinson, K.D., Deshpande, S. and Larsen, C.N. (1992) Comparisons of neuronal (PGP 9.5) and non-neuronal ubiquitin C-terminal hydrolases. *Biochem. Soc. Trans.*, **20**, 631–637.
8. Lowe, J., McDermott, H., Landon, M., Mayer, R.J. and Wilkinson, K.D. (1990) Ubiquitin carboxyl-terminal hydrolase (PGP 9.5) is selectively present in ubiquitinated inclusion bodies characteristic of human neurodegenerative diseases. *J. Pathol.*, **161**, 153–160.
9. Leroy, E., Boyer, R., Auburger, G., Leube, B., Ulm, G., Mezey, E., Harta, G., Brownstein, M.J., Jonnalagada, S., Chernova, T. *et al.* (1998) The ubiquitin pathway in Parkinson's disease. *Nature*, **395**, 451–452.
10. Saigoh, K., Wang, Y.L., Suh, J.G., Yamanishi, T., Sakai, Y., Kiyosawa, H., Harada, T., Ichihara, N., Wakana, S., Kikuchi, T. *et al.* (1999) Intragenic deletion in the gene encoding ubiquitin carboxy-terminal hydrolase in *gad* mice. *Nat. Genet.*, **23**, 47–51.
11. Kikuchi, T., Mukoyama, M., Yamazaki, K. and Moriya, H. (1990) Axonal degeneration of ascending sensory neurons in gracile axonal dystrophy mutant mouse. *Acta. Neuropathol. (Berl.)*, **80**, 145–151.
12. Wilkinson, K.D. (1997) Regulation of ubiquitin-dependent processes by deubiquitinating enzymes. *FASEB J.*, **11**, 1245–1256.
13. Liu, Y., Fallon, L., Lashuel, H.A., Liu, Z. and Lansbury, P.T. (2002) The UCH-L1 gene encodes two opposing enzymatic activities that affect alpha-synuclein degradation and Parkinson's disease susceptibility. *Cell*, **111**, 209–218.
14. Johnston, S.C., Larsen, C.N., Cook, W.J., Wilkinson, K.D. and Hill, C.P. (1997) Crystal structure of a deubiquitinating enzyme (human UCH-L3) at 1.8 Å resolution. *EMBO J.*, **16**, 3787–3796.
15. Morimoto, T., Ide, T., Ihara, Y., Tamura, A. and Kirino, T. (1996) Transient ischemia depletes free ubiquitin in the gerbil hippocampal CA1 neurons. *Am. J. Pathol.*, **148**, 249–257.
16. Takada, K., Hibi, N., Tsukada, Y., Shibasaki, T. and Ohkawa, K. (1996) Ability of ubiquitin radioimmunoassay to discriminate between mono-ubiquitin and multi-ubiquitin chains. *Biochim. Biophys. Acta*, **1290**, 282–288.
17. Fujimuro, M., Sawada, H. and Yokosawa, H. (1994) Production and characterization of monoclonal antibodies specific to multi-ubiquitin chains of polyubiquitinated proteins. *FEBS Lett.*, **349**, 173–180.
18. Takada, K., Nasu, H., Hibi, N., Tsukada, Y., Ohkawa, K., Fujimuro, M., Sawada, H. and Yokosawa, H. (1995) Immunoassay for the quantification of intracellular multi-ubiquitin chains. *Eur. J. Biochem.*, **233**, 42– 47.
19. Swaminathan, S., Amerik, A.Y. and Hochstrasser, M. (1999) The Doa4 deubiquitinating enzyme is required for ubiquitin homeostasis in yeast. *Mol. Biol. Cell*, **10**, 2583–2594.
20. Amerik, A.Y., Nowak, J., Swaminathan, S. and Hochstrasser, M. (2000) The Doa4 deubiquitinating enzyme is functionally linked to the vacuolar protein-sorting and endocytic pathways. *Mol. Biol. Cell*, **11**, 3365–3380.
21. Johnston, S.C., Riddle, S.M., Cohen, R.E. and Hill, C.P. (1999) Structural basis for the specificity of ubiquitin C-terminal hydrolases. *EMBO J.*, **18**, 3877–3887.
22. Shih, S.C., Sloper-Mould, K.E. and Hicke, L. (2000) Monoubiquitin carries a novel internalization signal that is appended to activated receptors. *EMBO J.*, **19**, 187–198.
23. Nakatsu, F., Sakuma, M., Matsuo, Y., Arase, H., Yamasaki, S., Nakamura, N., Saito, T. and Ohno, H. (2000) A di-leucine signal in the ubiquitin moiety. Possible involvement in ubiquitination-mediated endocytosis. *J. Biol. Chem.*, **275**, 26213–26219.
24. Bennett, M.C., Bishop, J.F., Leng, Y., Chock, P.B., Chase, T.N. and Mouradian, M.M. (1999) Degradation of alpha-synuclein by proteasome. *J. Biol. Chem.*, **274**, 33855–33858.
25. Rochet, J.C. and Lansbury, P.T. Jr (2000) Amyloid fibrillogenesis: themes and variations. *Curr. Opin. Struct. Biol.*, **10**, 60–68.
26. Shimura, H., Hattori, N., Kubo, S., Mizuno, Y., Asakawa, S., Minoshima, S., Shimizu, N., Iwai, K., Chiba, T., Tanaka, K. *et al.* (2000) Familial Parkinson disease gene product, parkin, is a ubiquitin-protein ligase. *Nat. Genet.*, **25**, 302–305.
27. Imai, Y., Soda, M., Inoue, H., Hattori, N., Mizuno, Y. and Takahashi, R. (2001) An unfolded putative transmembrane polypeptide, which can lead to endoplasmic reticulum stress, is a substrate of Parkin. *Cell*, **105**, 891–902.

28. Bizzi, A., Schaetzle, B., Patton, A., Gambetti, P. and Autilio-Gambetti, L. (1991) Axonal transport of two major components of the ubiquitin system: free ubiquitin and ubiquitin carboxyl-terminal hydrolase PGP 9.5. *Brain Res.*, **548**, 292–299.
29. Momose, Y., Murata, M., Kobayashi, K., Tachikawa, M., Nakabayashi, Y., Kanazawa, I. and Toda, T. (2002) Association studies of multiple candidate genes for Parkinson's disease using single nucleotide polymorphisms. *Ann. Neurol.*, **51**, 133–136.
30. Satoh, J. and Kuroda, Y. (2001) A polymorphic variation of serine to tyrosine at codon 18 in the ubiquitin C-terminal hydrolase-L1 gene is associated with a reduced risk of sporadic Parkinson's disease in a Japanese population. *J. Neurol. Sci.*, **189**, 113–117.
31. Wang, J., Zhao, C.Y., Si, Y.M., Liu, Z.L., Chen, B. and Yu, L. (2002) ACT and UCH-L1 polymorphisms in Parkinson's disease and age of onset. *Mov. Disord.*, **17**, 767–771.
32. Maraganore, D.M., Farrer, M.J., Hardy, J.A., Lincoln, S.J., McDonnell, S.K. and Rocca, W.A. (1999) Case-control study of the ubiquitin carboxy-terminal hydrolase L1 gene in Parkinson's disease. *Neurology*, **53**, 1858–1860.
33. Polymeropoulos, M.H., Lavedan, C., Leroy, E., Ide, S.E., Dehejia, A., Dutra, A., Pike, B., Root, H., Rubenstein, J., Boyer, R. *et al.* (1997) Mutation in the alpha-synuclein gene identified in families with Parkinson's disease. *Science*, **276**, 2045–2047.
34. Kitada, T., Asakawa, S., Hattori, N., Matsumine, H., Yamamura, Y., Minoshima, S., Yokochi, M., Mizuno, Y. and Shimizu, N. (1998) Mutations in the parkin gene cause autosomal recessive juvenile parkinsonism. *Nature*, **392**, 605–608.
35. Bonifati, V., Rizzu, P., Van Baren, M.J., Schaap, O., Breedveld, G.J., Krieger, E., Dekker, M.C., Squitieri, F., Ibanez, P., Joosse, M. *et al.* (2002) Mutations in the DJ-1 gene associated with autosomal recessive early-onset Parkinsonism. *Science.* Published online 21 November 2002; 10.1126/science.1077209.
36. Shimura, H., Schlossmacher, M.G., Hattori, N., Frosch, M.P., Trockenbacher, A., Schneider, R., Mizuno, Y., Kosik, K.S. and Selkoe, D.J. (2001) Ubiquitination of a new form of alpha-synuclein by parkin from human brain: implications for Parkinson's disease. *Science*, **293**, 263–269.
37. Abeliovich, A., Schmitz, Y., Farinas, I., Choi-Lundberg, D., Ho, W.H., Castillo, P.E., Shinsky, N., Verdugo, J.M., Armanini, M., Ryan, A. *et al.* (2000) Mice lacking alpha-synuclein display functional deficits in the nigrostriatal dopamine system. *Neuron*, **25**, 239–252.
38. Kurihara, L.J., Semenova, E., Levorse, J.M. and Tilghman, S.M. (2000) Expression and functional analysis of Uch-L3 during mouse development. *Mol. Cell. Biol.*, **20**, 2498–2504.

American Journal of Pathology, Vol. 164, No. 1, January 2004
Copyright © American Society for Investigative Pathology

Role of Ubiquitin Carboxy Terminal Hydrolase-L1 in Neural Cell Apoptosis Induced by Ischemic Retinal Injury *in Vivo*

Takayuki Harada,*† Chikako Harada,*† Yu-Lai Wang,* Hitoshi Osaka,*‡ Kazuhito Amanai,† Kohichi Tanaka,†‡ Shuichi Takizawa,* Rieko Setsuie,*§ Mikako Sakurai,*§ Yae Sato,*§ Mami Noda,§ and Keiji Wada*

From the Department of Degenerative Neurological Diseases, National Institute of Neuroscience, National Center of Neurology and Psychiatry, Kodaira, Tokyo; Laboratory of Molecular Neuroscience,† School of Biomedical Science and Medical Research Institute, Tokyo Medical and Dental University, Tokyo; Precursory Research for Embryonic Science and Technology (PRESTO),‡ Japan Science and Technology Corporation (JST), Kawaguchi, Saitama; Laboratory of Pathophysiology,§ Graduate School of Pharmaceutical Sciences, Kyushu University, Higashi-ku, Fukuoka, Japan*

Ubiquitin is thought to be a stress protein that plays an important role in protecting cells under stress conditions; however, its precise role is unclear. Ubiquitin expression level is controlled by the balance of ubiquitinating and deubiquitinating enzymes. To investigate the function of deubiquitinating enzymes on ischemia-induced neural cell apoptosis *in vivo*, we analyzed gracile axonal dystrophy (*gad*) mice with an exon deletion for ubiquitin carboxy terminal hydrolase-L1 (UCH-L1), a neuron-specific deubiquitinating enzyme. In wild-type mouse retina, light stimuli and ischemic retinal injury induced strong ubiquitin expression in the inner retina, and its expression pattern was similar to that of UCH-L1. On the other hand, *gad* mice showed reduced ubiquitin induction after light stimuli and ischemia, whereas expression levels of antiapoptotic (Bcl-2 and XIAP) and prosurvival (brain-derived neurotrophic factor) proteins that are normally degraded by an ubiquitin-proteasome pathway were significantly higher. Consistently, ischemia-induced caspase activity and neural cell apoptosis were suppressed ~70% in *gad* mice. These results demonstrate that UCH-L1 is involved in ubiquitin expression after stress stimuli, but excessive ubiquitin induction following ischemic injury may rather lead to neural cell apoptosis *in vivo*. *(Am J Pathol 2004, 164:59–64)*

The small 76 amino acid protein ubiquitin plays a critical role in many cellular processes, including cell cycle control, transcriptional regulation, and synaptic development.[1,2] Although ubiquitin has been identified as a heat shock- and stress-regulated protein in several kinds of cells,[3,4] recent studies have shown that ubiquitin promotes either cell survival or apoptosis, depending on the stage of cell development or other cellular factors.[5–8] Ubiquitin expression level is controlled by the balance of ubiquitinating enzymes: ubiquitin-activating (E1), ubiquitin-conjugating (E2), ubiquitin-ligase (E3) enzymes, and deubiquitinating enzymes (DUBs). DUBs are subdivided into ubiquitin carboxy terminal hydrolases (UCHs) and ubiquitin-specific proteases (UBPs). Mammalian UCHs, UCH-L1, and UCH-L3 are both small proteins of ~220 amino acids that share >40% amino acid sequence identity.[9] However, the distribution of these isozymes is quite distinct in that UCH-L3 is distributed ubiquitously while UCH-L1 is selectively expressed in neuronal cells and in the testis/ovary.[9,10] UCH-L1 constitutes ~5% of the brain's total soluble protein, which demonstrates a possibility that it plays a major role in neuronal cell function.[11] Indeed, UCH-L1 is a constituent of cellular aggregates that are indicative of neurodegenerative disease, such as Lewy bodies in Parkinson's disease.[12] Furthermore, an isoleucine to methionine substitution at amino acid 93 of UCH-L1 is reported in a family with a dominant form of Parkinson's disease.[13] Recently, we found a UCH-L1 gene exon deletion in mice that causes gracile axonal dystrophy (*gad*), a recessive neurodegenerative disease.[14] These examples of neurodysfunction from UCH-L1 mutations in both humans and mice prompted us to investigate the function of UCH-L1 in ischemia-induced neuronal cell apoptosis. For this purpose, we evaluated the extent of ischemic injury in wild-type and *gad* mice retina. The retina was chosen as a model be-

Supported by grants from the Organization for Pharmaceutical Safety and Research, Japan Science and Technology Cooperation, the Ministry of Health, Labor and Welfare of Japan, and the Ministry of Education, Culture, Sports, Science and Technology of Japan.

C. H. was supported by the Japan Society for the Promotion of Science for Young Scientists.

Accepted for publication September 10, 2003.

Address reprint requests to Keiji Wada, M.D., Ph.D., Department of Degenerative Neurological Diseases, National Institute of Neuroscience, NCNP, 4-1-1 Ogawahigashi, Kodaira, Tokyo 187-8502, Japan. E-mail: wada@ncnp.go.jp.

cause it is a highly organized neural tissue. In addition, its layered construction is suitable for analysis of cell type-specific biological response against diverse stimuli.[15–18] Here, we show that the absence of UCH-L1 partially prevents ischemia-induced retinal cell apoptosis and propose its possible mechanisms.

Materials and Methods

Animals

We used homozygous *gad* mice[14] and their wild-type littermates between postnatal days 35 and 56. The *gad* mouse was found in the F2 offspring of CBA and RFM inbred strain mice and has been maintained by brother-sister mating for more than 10 years.[19] Mice were maintained and propagated at the National Institute of Neuroscience, National Center of Neurology and Psychiatry (Japan). Experiments using the mice were approved by the Animal Investigation Committee of the Institute. The animals were housed in a room with controlled temperature and fixed lighting schedule. Light intensity inside the cages ranged from 100 to 200 lux. For the analysis of light stress, the pupils were dilated with 0.5% phenylephrin-ezhydrochloride and 0.5% tropicamide, and the mice were exposed to 800~1300 lux of white fluorescent light for 30 minutes. Animals for negative controls were dark-adapted for 12 hours, and sacrificed under dim red light.

Immunohistochemistry

Animals were anesthetized with diethylether and perfused transcardially with saline, followed by 4% paraformaldehyde in 0.1 mol/L phosphate buffer containing 0.5% picric acid at room temperature. The eyes were removed and postfixed overnight in the same fixative at 4°C and embedded in paraffin wax. The posterior part of the eyes were sectioned saggitally at 7-μm thickness through the optic nerve, mounted and stained with hematoxylin and eosin. For immunohistochemical staining, the sections were incubated with phosphate-buffered saline (PBS) containing 10% normal donkey serum for 30 minutes at room temperature. They were then incubated overnight with a rabbit polyclonal antibody against ubiquitin (1:600; Chemicon, Temecula, CA) or mouse monoclonal antibody against UCH-L1 (1:200; Medac, Wedel, Germany). They were then visualized with fluorescein isothiocyanate (FITC)-conjugated goat anti-rabbit or anti-mouse IgG (Jackson Immunoresearch, West Grove, PA), respectively. The sections were examined by a confocal laser scanning microscope (Olympus, Tokyo, Japan).

Histology and Morphometric Studies

Ischemia was achieved and the animals were sacrificed as previously described.[16,17] Briefly, we instilled sterile saline into the anterior chamber of the left eye at 150 cm H_2O pressure for 15 minutes while the right eye served as a non-ischemic control. The animals were sacrificed 1 or 7 days after reperfusion, and eyes were enucleated for histological and morphometric studies. The posterior part of the eyes was sectioned sagittally at 7-μm thickness through the optic nerve, mounted and stained with hematoxylin and eosin. Ischemic damage after 7 days was quantified in two ways. First, the thickness of the inner retinal layer (IRL) [from the ganglion cell layer (GCL) to the inner nuclear layer (INL)] was measured with a calibrated reticle at ×80. Second, in the same sections, the number of cells in the GCL was counted from one ora serrata through the optic nerve to the other ora serrata. The changes of the number of ganglion cells after ischemia were expressed in ratio compared with the non-ischemic fellow eyes.

TUNEL Staining

Sections were incubated in 0.26 U/μl TdT in the supplied 1X buffer (Invitrogen, Carlsbad, CA), and 20 μmol/L biotinylated-16-dUTP (Roche, Basel, Switzerland) for 60 minutes at 37°C. Sections were washed three times in PBS (pH 7.4) and blocked for 30 minutes with 2% bovine serum albumin in PBS (pH 7.4). The sections were then incubated with FITC-coupled streptavidin (Jackson Immunoresearch), diluted 1:100 in PBS for 30 minutes, and examined with a confocal laser scanning microscope (Olympus).

Quantification of Retinal Cell Apoptosis and Caspase Activities

A mouse retina 1 day after ischemia was homogenized in 100 μl PBS containing 1 mmol/L phenylmethyl sulfonyl fluoride and centrifuged at 15,000 × *g* for 10 minutes. A portion of supernatant was used to quantify protein concentration, and the rest was processed for assays. Retinal cell apoptosis was quantified using the Cell Death ELISA kit (Roche). Caspase-1- and caspase-3-like activities were measured using caspase-1 and caspase-3 Colorimetric Assay Kits (Bio-vision, Mountain View, CA), respectively.

Western Blot Analysis

Western blots were performed as previously reported.[14] Five micrograms of total protein were loaded per lane. Primary antibodies used were Bcl-2 (1:500), Bcl-xL (1:500), XIAP (1:500) (all from Transduction Laboratories, Franklin Lakes, NJ), phosphorylated cyclic AMP responsive element-binding protein (PCREB) (1:500; Upstate Biotechnology, Waltham, MA) and brain-derived neurotrophic factor (BDNF) (1:500; Santa Cruz Biotechnology, Santa Cruz, CA). Blots were further incubated with an anti-mouse or rabbit IgG-horseradish peroxidase conjugate (1:10000; Chemicon). The Super Signal detection kit (Pierce, Rockford, IL) was used for visualization of immunoreactive bands.

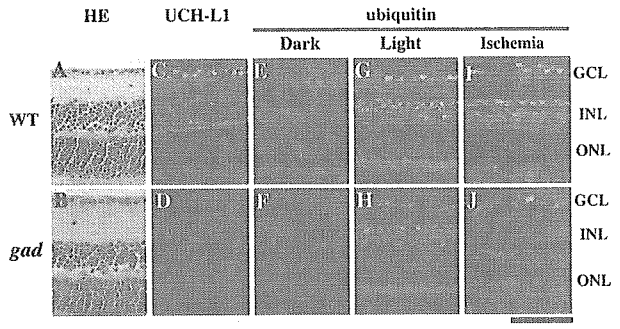

Figure 1. Functional loss of UCH-L1 decreases light- and ischemia-induced ubiquitin induction *in vivo*. Hematoxylin and eosin (HE) staining (**A** and **B**), immunostaining of UCH-L1 (**C** and **D**), immunostaining of ubiquitin in dark-reared (**E** and **F**), light-stressed (**G** and **H**) and ischemic (**I** and **J**) retina in wild-type (**A**, **C**, **E**, **G**, and **I**) and *gad* (**B**, **D**, **F**, **H**, and **J**) mice. Retinal structure is normal (**B**), but stress-induced ubiquitin induction is reduced (**H** and **J**) in *gad* mice. For the analysis of light stress (**G** and **H**), mice were exposed to 800 to 1300 lux of light for 30 minutes. Animals for negative controls were dark-adapted for 12 hours, and sacrificed under dim red light (**E** and **F**). Ischemic retina was prepared 1 day after ischemic injury (**I** and **J**). Bar, 50 μm.

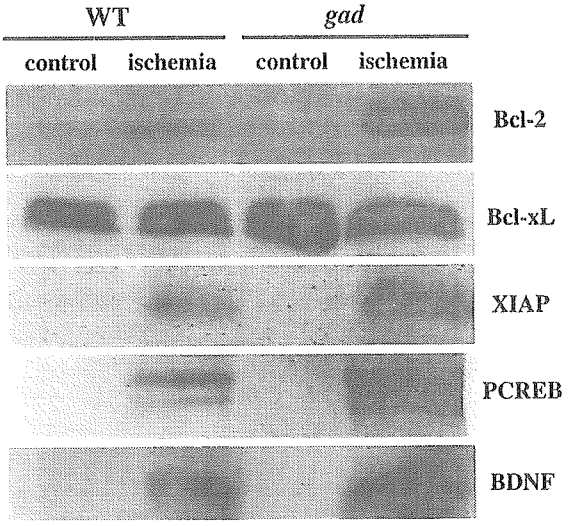

Figure 2. Immunoblot analysis of antiapoptotic and prosurvival proteins after ischemic injury. Five micrograms of total protein were prepared from whole retinas before (control) and 1 day after ischemic injury (ischemia). Representative image of four independent experiments are shown.

Results

Effect of UCH-L1 on Retinal Structure and Ubiquitin Expression

To determine the effect of UCH-L1 on retinal morphology, we examined the retinal tissue of *gad* mice with a UCH-L1 gene exon deletion.[14] Retinal structure in *gad* mice (Figure 1B) was normal compared with wild-type mice (Figure 1A). UCH-L1-like immunoreactivity was observed in the ganglion cell layer (GCL) and the inner nuclear layer (INL) in wild-type mice (Figure 1C) but was absent in *gad* mice (Figure 1D). Since ubiquitin is thought to be a stress protein,[1,20] we first examined the effect of the common oxidative stress for eye tissues, light stimuli, on ubiquitin induction.[20] Interestingly, ubiquitin was almost absent in both groups of animals, following dark adaptation (Figure 1, E and F). However, light stimuli strongly induced ubiquitin expression in the GCL and INL in wild-type mice (Figure 1G) but its induction level was very low in *gad* mice (Figure 1H). Ubiquitin expression pattern in wild-type mice was similar to that of UCH-L1 (Figure 1C). We next examined the effect of ischemia, severe oxidative stress,[21,22] on ubiquitin induction. As with light stimuli, ischemia induced strong ubiquitin expression in the GCL and INL (Figure 1I) and its induction was suppressed in *gad* mice (Figure 1J). These results demonstrate that retinal UCH-L1 plays an important role in ubiquitin induction[11] and *gad* mice retina is a useful model to investigate the effects of UCH-L1 on ischemic injury *in vivo*.

Effect of UCH-L1 on Antiapoptotic and Prosurvival Protein Expressions Following Ischemic Injury

The ubiquitin-proteasome pathway might be involved in non-neural cell apoptosis because this pathway can degradate antiapoptotic proteins such as Bcl-2 and XIAP *in vitro*.[5–8] To determine whether this is true for retinal cell apoptosis *in vivo*, we examined their protein expression levels in ischemic retinas (Figure 2). Ischemia-induced Bcl-2 protein level in *gad* mice was substantially higher than that of wild-type mice. Bcl-xL proteins (antiapoptotic member in the Bcl-2 family)[23,24] were examined at the same time as a control, but no obvious alternations were noted. On the other hand, XIAP protein[25,26] expression was apparently higher in *gad* mice. In addition to oxidative stress, ischemia induces calcium influx in neurons and triggers phosphorylation of cyclic AMP responsive element-binding protein (CREB).[27] PCREB can activate transcription of trophic factor proteins, such as BDNF, by binding to a critical calcium response element.[27] Since CREB is degraded by a ubiquitin-proteasome pathway by a phosphorylation-dependent mechanism,[28] we hypothesized a similar degradative pathway for CREB in ischemic retina. In wild-type mice, ischemia increased PCREB, but its expression level was much higher in *gad* mice. Consistent with PCREB up-regulation, BDNF protein expression was also higher in *gad* mice. Thus, excessive ubiquitin induction after ischemic injury may lead to the degradation of antiapoptotic proteins and suppression of the transcription of prosurvival proteins.[5–8,28]

Effect of UCH-L1 on Ischemia-Induced Neural Cell Apoptosis

To determine whether increased expression of antiapoptotic and prosurvival proteins in *gad* mice really leads to resistance against ischemia, we next examined the histology of ischemic retinas in both strains. As expected, ischemic damage in *gad* mice was mild compared with wild-type mice (Figure 3); the thickness of the inner retinal layer (IRL) (Figure 4A) and the percentage of surviving cells in the GCL (Figure 4B) after ischemia were significantly larger in *gad* mice. We also analyzed apoptotic cells in the retina by TUNEL staining. Control animals

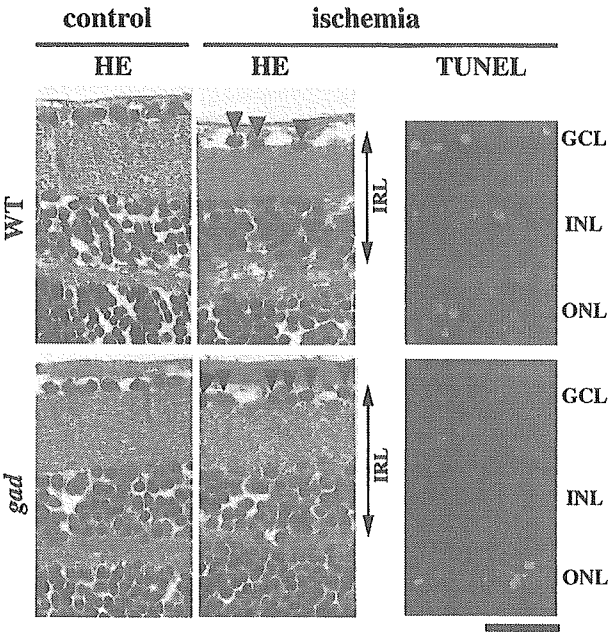

Figure 3. Representative pictures of HE staining (**left**) and TUNEL staining (**right**) in wild-type and *gad* mice retina before (control) and after ischemic injury (ischemia). Retinal damage 7 days after ischemia (HE staining) in *gad* mice was mild compared with wild-type mice. Consistently, TUNEL-positive cells 1 day after ischemia were observed only in the ONL in *gad* mice. Bar, 50 μm.

showed practically no signals in both strains (data not shown). However, in ischemic retinas, TUNEL-positive cells were observed in all three nuclear layers in wild-type mice, but mainly only in the outer nuclear layer (ONL) in *gad* mice (Figure 3). Consistently, quantitative analysis by ELISA demonstrated decreased retinal cell apoptosis in *gad* mice (Figure 4C). Ischemia-induced retinal cell apoptosis is executed by two distinct caspase proteases.

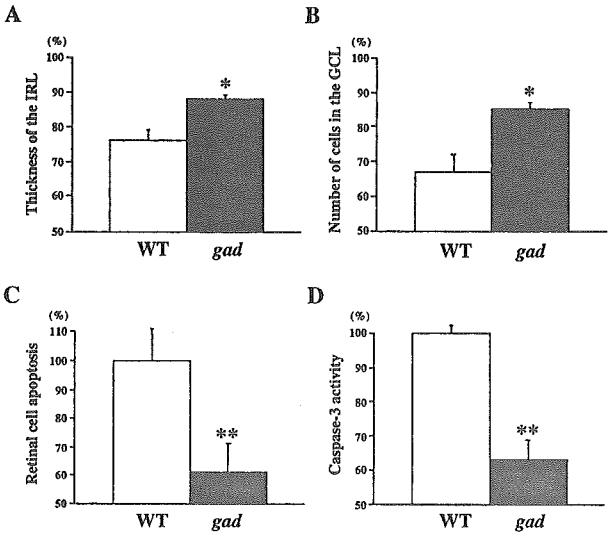

Figure 4. Effect of ischemic injury in wild-type and *gad* mice retina. Thickness of the IRL (arrows in Figure 3) (**A**) and the number of cells in the GCL (arrowheads in Figure 3) (**B**) in retina 7 days after ischemic injury as a percentage of the non-ischemic fellow eye. Quantitative analysis of retinal cell apoptosis (**C**) and caspase-3-like activity (**D**) in retina 1 day after ischemic injury. Results of six independent experiments are presented as mean ± SD (*, $P < 0.05$; **, $P < 0.01$).

Caspase-1 is predominantly associated with photoreceptor cell apoptosis in the ONL, whereas caspase-3 is more active in the GCL and INL for the same process.[29] To determine the mechanisms of strong tolerance against ischemia in *gad* mice, we next examined the activity of these two caspases in the ischemic retina. Caspase-1-like activity was not significantly different in *gad* mice compared with wild-type mice (80 ± 13%; P = not significant) (data not shown). On the other hand, caspase-3-like activity in *gad* mice was suppressed to 63 ± 6% compared with wild-type mice ($P < 0.01$) (Figure 4D).

Discussion

Ischemic injury is mainly associated with excessive concentrations of glutamate, which results in overactivation of glutamate receptors and initiates a cascade of events that leads to necrosis and/or apoptosis. Consistently, several studies have shown that retinal neurons can be protected by glutamate receptor antagonists.[17,30,31] An alternative strategy to attenuate glutamate neurotoxicity is keeping the extracellular glutamate concentration below neurotoxic levels. We previously demonstrated that selective inhibition of N-acetylated-α-linked-acidic dipeptidase (NAALADase), an enzyme responsible for the hydrolysis of neuropeptide N-acetyl-aspartyl-glutamate to N-acetyl-aspartate and glutamate, robustly protects neurons in a rat model of stroke[32] and in a mouse model of ischemic retinal injury.[17] Another possible target is the glutamate transporter.[33] There are four subtypes of glutamate transporters (GLAST, GLT-1, EAAC1, and EAAT5) in the retina.[16,33] By using GLAST and GLT-1 knockout mice,[34,35] we showed that both GLAST and GLT-1 (GLAST > GLT-1) are crucial for the protection of retinal cells from ischemic injury.[16]

In addition to these typical molecules involved in glutamate neurotoxicity, we first demonstrated that neuron-specific deubiquitinating enzyme, UCH-L1, is a new possible therapeutic target for ischemic retinal injury. In *gad* mice, functional loss of UCH-L1 results in the protection of retinal neurons following ischemic injury. One of the possible mechanisms is the accumulation of antiapoptotic proteins Bcl-2 and XIAP. Suppression of Bcl-2 leads to altered mitochondrial membrane permeability resulting in release of cytochrome c into the cytosol, which can trigger caspase activation leading to apoptosis.[23–26] On the other hand, a member of the IAP (inhibitor of apoptosis proteins) family, XIAP, can bind to and inhibit caspase-3 activation.[23–26] Consistently, retinal cell apoptosis in *gad* mice is suppressed mainly in the inner retina (Figure 3), where caspase-3 is more active than caspase-1.[27] These results suggest a possibility that functional loss of UCH-L1 may lead to decreased cytochrome c release from mitochondria and subsequent caspase inactivation in *gad* mice. If UCH-L1 inhibition works on the apoptotic pathway both before and after cytochrome c release from mitochondria,[23–26] this method may have a broader effect compared with the overexpression or suppression of a single antiapoptotic or apoptotic factor, respectively.

On the other hand, BDNF and PCREB protein expression levels were also up-regulated in *gad* mice. Recent studies have shown that trophic factors such as BDNF, ciliary neurotrophic factor (CNTF), basic fibroblast growth factor (bFGF), or glial cell line-derived neurotrophic factor (GDNF) increase RGC survival and regeneration.[36–45] Since CREB plays a central role in mediating responses of trophic factors including BDNF,[27] enhanced release of these trophic factors in *gad* mice may prevent ischemia-induced retinal cell apoptosis. We previously showed that, in addition to direct neuroprotection, these factors can alter secondary trophic factor production in retina-specific Müller glial cells, which indirectly regulate neural cell survival.[18,46] Consistently, intraocular injection of trophic factors induces the phosphorylated form of extracellular receptor kinase (pERK) or c-fos mainly in Müller cells.[47,48] Thus, loss of UCH-L1 may induce neural cell survival by stimulating both neural and glial cells.[18,46,49]

Ischemic retinal injury is implicated in a number of pathological states, such as retinal artery occlusion, glaucoma, and diabetic retinopathy.[16,17,30,31] Accordingly, the present results raise intriguing possibilities for the management of these pathological conditions by modifying the expression of UCH-L1 and activity of the ubiquitin-proteasome pathway.[50] Using this strategy with trophic factors,[18,46] NAALADase inhibitor,[17] glutamate transporter activators, such as bromocryptine,[51,52] or overexpression of GLAST or GLT-1,[16] may induce synergic effects on multiple cellular targets to prevent ischemia-induced neural cell apoptosis. However, due to the central function of the ubiquitin system in many basic cellular processes, modulation of this system can become a "double-edged sword".[1] Depletion of the free ubiquitin pool may cause accumulation of proteins that should be subjected to ubiquitin-dependent proteolysis. To address these critical issues, further investigations revealing the functional site of UCH-L1 and its involvement in ubiquitin induction *in vivo* will be needed.

Acknowledgments

We thank H.-M. A. Quah and L.F. Parada for critical reading of the manuscript, and members of the Wada lab for helpful discussions.

References

1. Hershko A, Ciechanover A, Varshavsky A: The ubiquitin system. Nat Med 2000, 6:1073–1081
2. DiAntonio A, Haghighi AP, Portman SL, Lee JD, Amaranto AM, Goodman CS: Ubiquitination-dependent mechanisms regulate synaptic growth and function. Nature 2001, 412:449–452
3. Finley D, Ozkaynak E, Varshavsky A: The yeast polyubiquitin gene is essential for resistance to high temperatures, starvation, and other stresses. Cell 1987, 48:1035–1046
4. Bond U, Agell N, Haas AL, Redman K, Schlesinger MJ: Ubiquitin in stressed chicken embryo fibroblasts. J Biol Chem 1988, 263:2384–2388
5. Dimmeler S, Breitschopf K, Haendeler J, Zeiher AM: Dephosphorylation targets Bcl-2 for ubiquitin-dependent degradation: a link between the apoptosome and the proteasome pathway. J Exp Med 1999, 189:1815–1822
6. Breitschopf K, Haendeler J, Malchow P, Zeiher AM, Dimmeler S: Posttranslational modification of Bcl-2 facilitates its proteasome-dependent degradation: molecular characterization of the involved signaling pathway. Mol Cell Biol 2000, 20:1886–1896
7. Daino H, Matsumura I, Takada K, Odajima J, Tanaka H, Ueda S, Shibayama H, Ikeda H, Hibi M, Machii T, Hirano T, Kanakura Y: Induction of apoptosis by extracellular ubiquitin in human hematopoietic cells: possible involvement of STAT3 degradation by proteasome pathway in interleukin 6-dependent hematopoietic cells. Blood 2000, 95:2577–2585
8. Yang Y, Fang S, Jensen JP, Weissman AM, Ashwell JD: Ubiquitin protein ligase activity of IAPs and their degradation in proteasomes in response to apoptotic stimuli. Science 2000, 288:874–877
9. Wilkinson KD, Lee KM, Deshpande S, Duerksen-Hughes P, Boss JM, Pohl J: The neuron-specific protein PGP 9.5 is a ubiquitin carboxyl-terminal hydrolase. Science 1989, 246:670–673
10. Wilkinson KD, Deshpande S, Larsen CN: Comparisons of neuronal (PGP 9.5) and non-neuronal ubiquitin C-terminal hydrolases. Biochem Soc Trans 1992, 20:631–637
11. Osaka H, Wang YL, Takada K, Takizawa S, Setsuie R, Li H, Sato Y, Nishikawa K, Sun YJ, Sakurai M, Harada T, Hara Y, Kimura I, Chiba S, Namikawa K, Kiyama H, Noda M, Aoki S, Wada K: Ubiquitin carboxy-terminal hydrolase L1 binds to and stabilizes monoubiquitin in neuron. Hum Mol Genet 2003, 12:1945–1958
12. Lowe J, McDermott H, Landon M, Mayer RJ, Wilkinson KD: Ubiquitin carboxyl-terminal hydrolase (PGP 9.5) is selectively present in ubiquitinated inclusion bodies characteristic of human neurodegenerative diseases. J Pathol 1990, 161:153–160
13. Leroy E, Boyer R, Auburger G, Leube B, Ulm G, Mezey E, Harta G, Brownstein MJ, Jonnalagada S, Chernova T, Dehejia A, Lavedan C, Gasser T, Steinbach PJ, Wilkinson KD, Polymeropoulos MH: The ubiquitin pathway in Parkinson's disease. Nature 1998, 395:451–452
14. Saigoh K, Wang YL, Suh JG, Yamanishi T, Sakai Y, Kiyosawa H, Harada T, Ichihara N, Wakana S, Kikuchi T, Wada K: Intragenic deletion in the gene encoding ubiquitin carboxy-terminal hydrolase in gad mice. Nat Genet 1999, 23:47–51
15. Harada T, Imaki J, Hagiwara M, Ohki K, Takamura M, Ohashi T, Matsuda H, Yoshida K: Phosphorylation of CREB in rat retinal cells after focal retinal injury. Exp Eye Res 1995, 61:769–772
16. Harada T, Harada C, Watanabe M, Inoue Y, Sakagawa T, Nakayama N, Sasaki S, Okuyama S, Watase K, Wada K, Tanaka K: Functions of the two glutamate transporters GLAST and GLT-1 in the retina. Proc Natl Acad Sci USA 1998, 95:4663–4666
17. Harada C, Harada T, Slusher BS, Yoshida K, Matsuda H, Wada K: N-acetylated-α-linked-acidic dipeptidase inhibitor has a neuroprotective effect on mouse retinal ganglion cells after pressure-induced ischemia. Neurosci Lett 2000, 292:134–136
18. Harada T, Harada C, Nakayama N, Okuyama S, Yoshida K, Kohsaka S, Matsuda H, Wada K: Modification of glial-neuronal cell interactions prevents photoreceptor apoptosis during light-induced retinal degeneration. Neuron 2000, 26:533–541
19. Yamazaki K, Wakasugi N, Tomita T, Kikuchi T, Mukoyama M, Ando K: Gracile axonal dystrophy (GAD), a new neurological mutant in the mouse. Proc Soc Exp Biol Med 1988, 187:209–215
20. Naash MI, Al-Ubaidi MR, Anderson RE: Light exposure induces ubiquitin conjugation and degradation activities in the rat retina. Invest Ophthalmol Vis Sci 1997, 38:2344–2354
21. Bonfoco E, Krainc D, Ankarcrona M, Nicotera P, Lipton SA: Apoptosis and necrosis: two distinct events induced, respectively, by mild and intense insults with N-methyl-D-aspartate or nitric oxide/superoxide in cortical cell cultures. Proc Natl Acad Sci USA 1995, 92:7162–7166
22. Szabo ME, Haines D, Garay E, Chiavaroli C, Farine JC, Hannaert P, Berta A, Garay RP: Antioxidant properties of calcium dobesilate in ischemic/reperfused diabetic rat retina. Eur J Pharmacol 2001, 428:277–286
23. Tsujimoto Y, Shimizu S: Bcl-2 family: life-or-death switch. FEBS Lett 2000, 466:6–10
24. Ranger AM, Malynn BA, Korsmeyer SJ: Mouse models of cell death. Nat Genet 2001, 28:113–118
25. Deveraux QL, Reed JC: IAP family proteins: suppressors of apoptosis. Genes Dev 1999, 13:239–252
26. Green DR: Apoptotic pathways: paper wraps stone blunts scissors. Cell 2000, 102:1–4

27. Finkbeiner S: CREB couples neurotrophin signals to survival messages. Neuron 2000, 25:11–14
28. Taylor CT, Furuta GT, Synnestvedt K, Colgan SP: Phosphorylation-dependent targeting of cAMP response element binding protein to the ubiquitin/proteasome pathway in hypoxia. Proc Natl Acad Sci USA 2000, 97:12091–12096
29. Katai N, Yoshimura N: Apoptotic retinal neuronal death by ischemia-reperfusion is executed by two distinct caspase family proteases. Invest Ophthalmol Vis Sci 1999, 40:2697–2705
30. Lipton SA: Retinal ganglion cells, glaucoma and neuroprotection. Prog Brain Res 2001, 131:712–718
31. Osborne NN, Melena J, Chidlow G, Wood JP: A hypothesis to explain ganglion cell death caused by vascular insults at the optic nerve head: possible implication for the treatment of glaucoma. Br J Ophthalmol 2001, 85:1252–1259
32. Slusher BS, Vornov JJ, Thomas AG, Hurn PD, Harukuni I, Bhardwaj A, Traystman RJ, Robinson MB, Britton P, Lu XC, Tortella FC, Wozniak KM, Yudkoff M, Potter BM, Jackson PF: Selective inhibition of NAALADase, which converts NAAG to glutamate, reduces ischemic brain injury. Nat Med 1999, 5:1396–1402
33. Tanaka K: Functions of glutamate transporters in the brain. Neurosci Res 2000, 37:15–19
34. Tanaka K, Watase K, Manabe T, Yamada K, Watanabe M, Takahashi K, Iwama H, Nishikawa T, Ichihara N, Kikuchi T, Okuyama S, Kawashima N, Hori S, Takimoto M, Wada K: Epilepsy and exacerbation of brain injury in mice lacking the glutamate transporter GLT-1. Science 1997, 276:1699–1702
35. Watase K, Hashimoto K, Kano M, Yamada K, Watanabe M, Inoue Y, Okuyama S, Sakagawa T, Ogawa S, Kawashima N, Hori S, Takimoto M, Wada K, Tanaka K: Motor discoordination and increased susceptibility to cerebellar injury in GLAST mutant mice. Eur J Neurosci 1998, 10:976–988
36. Mey J, Thanos S: Intravitreal injections of neurotrophic factors support the survival of axotomized retinal ganglion cells in adult rats in vivo. Brain Res 1993, 602:304–317
37. Cohen A, Bray GM, Aguayo AJ: Neurotrophin-4/5 (NT-4/5) increases adult rat retinal ganglion cell survival and neurite outgrowth in vitro. J Neurobiol 1994, 25:953–959
38. Mansour-Robaey S, Clarke DB, Wang YC, Bray GM, Aguayo AJ: Effects of ocular injury and administration of brain-derived neurotrophic factor on survival and regrowth of axotomized retinal ganglion cells. Proc Natl Acad Sci USA 1994, 91:1632–1636
39. Unoki K, LaVail MM: Protection of the rat retina from ischemic injury by brain-derived neurotrophic factor, ciliary neurotrophic factor, and basic fibroblast growth factor. Invest Ophthalmol Vis Sci 1994, 35: 907–915
40. Hammes HP, Federoff HJ, Brownlee M: Nerve growth factor prevents both neuroretinal programmed cell death and capillary pathology in experimental diabetes. Mol Med 1995, 1:527–534
41. Bosco A, Linden R: BDNF and NT-4 differentially modulate neurite outgrowth in developing retinal ganglion cells. J Neurosci Res 1999, 57:759–769
42. Yan Q, Wang J, Matheson CR, Urich JL: Glial cell line-derived neurotrophic factor (GDNF) promotes the survival of axotomized retinal ganglion cells in adult rats: comparison to and combination with brain-derived neurotrophic factor (BDNF). J Neurobiol 1999, 38:382–390
43. Di Polo A, Aigner LJ, Dunn RJ, Bray GM, Aguayo AJ: Prolonged delivery of brain-derived neurotrophic factor by adenovirus-infected Müller cells temporarily rescues injured retinal ganglion cells. Proc Natl Acad Sci USA 1998, 95:3978–3983
44. Koeberle PD, Ball AK: Neurturin enhances the survival of axotomized retinal ganglion cells in vivo: combined effects with glial cell line-derived neurotrophic factor and brain-derived neurotrophic factor. Neuroscience 2002, 110:555–567
45. Peterson WM, Wang Q, Tzekova R, Wiegand SJ: Ciliary neurotrophic factor and stress stimuli activate the Jak-STAT pathway in retinal neurons and glia. J Neurosci 2000, 20:4081–4090
46. Harada T, Harada C, Kohsaka S, Wada E, Yoshida K, Ohno S, Mamada H, Tanaka K, Parada LF, Wada K: Microglia-Müller glia cell interactions control neurotrophic factor production during light-induced retinal degeneration. J Neurosci 2002, 22:9228–9236
47. Wahlin KJ, Campochiaro PA, Zack DJ, Adler R: Neurotrophic factors cause activation of intracellular signaling pathways in Müller cells and other cells of the inner retina, but not photoreceptors. Invest Ophthalmol Vis Sci 2000, 41:927–936
48. Wahlin KJ, Adler R, Zack DJ, Campochiaro PA: Neurotrophic signaling in normal and degenerating rodent retinas. Exp Eye Res 2001, 73:693–701
49. Bringmann A, Reichenbach A: Role of Müller cells in retinal degenerations. Front Biosci 2001, 6:E72–E92
50. Nishikawa K, Li H, Kawamura R, Osaka H, Wang YL, Hara Y, Hirokawa T, Manago Y, Amano T, Noda M, Aoki S, Wada K: Alterations of structure and hydrolase activity of parkinsonism-associated human ubiquitin carboxyl-terminal hydrolase L1 variants. Biochem Biophys Res Commun 2003, 304:176–183
51. Yamashita H, Kawakami H, Zhang YX, Tanaka K, Nakamura S: Neuroprotective mechanism of bromocriptine. Lancet 1995, 346:1305
52. Yamashita H, Kawakami H, Zhang YX, Tanaka K, Nakamura S: Effect of amino acid ergot alkaloids on glutamate transport via human glutamate transporter hGluT-1. J Neurol Sci 1998, 155:31–36

Journal of Neurochemistry, 2004, **88**, 1540–1546 doi:10.1046/j.1471-4159.2003.02288.x

Proteomic analysis of brain proteins in the gracile axonal dystrophy (*gad*) mouse, a syndrome that emanates from dysfunctional ubiquitin carboxyl-terminal hydrolase L-1, reveals oxidation of key proteins

Alessandra Castegna,* Visith Thongboonkerd,** Jon Klein,** Bert C. Lynn,*†‡ Yu-Lai Wang,§ Hitoshi Osaka,§¶ Keiji Wada,§ and D. Allan Butterfield*‡

**Department of Chemistry and Center of Membrane Sciences, †Core Proteomics Laboratory and ‡Sanders-Brown Center on Aging, University of Kentucky, Lexington, Kentucky 40506 USA*

§Department of Degenerative Neurological Diseases, National Institute of Neuroscience, Tokyo, Japan

¶PRESTO, Japan Science and Technology Corporation, Saitama, Japan

***Kidney Disease Program and Proteomics Core Laboratory, University of Louisville, Louisville, Kentucky, USA*

Abstract

Ubiquitin carboxyl-terminal hydrolase L-1 (UCH L-1) is a crucial enzyme for proteasomal protein degradation that generates free monomeric ubiquitin. Our previous proteomic study identified UCH L-1 as one specific target of protein oxidation in Alzheimer's disease (AD) brain, establishing a link between the effect of oxidative stress on protein and the proteasomal dysfunction in AD. However, it is unclear how protein oxidation affects function, owing to the different responses of proteins to oxidation. Analysis of systems in which the oxidized protein displays lowered or null activity might be an excellent model for investigating the effect of the protein of interest in cellular metabolism and evaluating how the cell responds to the stress caused by oxidation of a specific protein. The gracile axonal dystrophy (*gad*) mouse is an autosomal recessive spontaneous mutant with a deletion on chromosome 5 within the gene encoding UCH L-1. The mouse displays axonal degeneration of the gracile tract. The aim of this proteomic study on *gad* mouse brain, with dysfunctional UCH L-1, was to determine differences in brain protein oxidation levels between control and *gad* samples. The results showed increased protein oxidation in thioredoxin peroxidase (peroxiredoxin), phosphoglycerate mutase, Rab GDP dissociation inhibitor α/ATP synthase and neurofilament-L in the *gad* mouse brain. These findings are discussed with reference to the effect of specific protein oxidation on potential mechanisms of neurodegeneration that pertain to the *gad* mouse.

Keywords: Alzheimer's disease, amyotrophic lateral sclerosis, brain protein oxidation, proteasome, proteomics, ubiquitin carboxyl terminal hydrolase L-1.

J. Neurochem. (2004) **88,** 1540–1546.

The gracile axonal dystrophy (*gad*) mouse is an autosomal recessive spontaneous mutant that was identified in 1984 (Yamazaki *et al.* 1988). Pathologically, the *gad* mouse displays axonal degeneration of the gracile tract, which consists of thoracic, lumbar and sacral dorsal root ganglion axons. This axonal deterioration results in progressive sensory ataxia, and eventually spreads to the motor neurons and other centers in the CNS, causing paralysis and death after 150 days of age (Yamazaki *et al.* 1988). Accumulation of ubiquitin and amyloid-β protein deposits is also present along the sensory and motor nervous system (Wu *et al.* 1996).

Received October 14, 2003; revised manuscript received November 18, 2003; accepted November 20, 2003.

Address correspondence and reprint requests to Professor D. Allan Butterfield, Department of Chemistry and Center of Membrane Sciences, University of Kentucky, Lexington, KY 40506-0055, USA.
E-mail: dabcns@uky.edu

Abbreviations used: AD, Alzheimer's disease; DNP, dinitrophenyl hydrazone; DNPH, 2,4-dinitrophenylhydrazine; 2D PAGE, two-dimensional polyacrylamide gel electrophoresis; IPG, immobilized pH gradient; MS/MS, tandem mass spectrometry; UCH L-1, ubiquitin carboxyl-terminal hydrolase L-1.

© 2004 International Society for Neurochemistry, *J. Neurochem.* (2004) **88**, 1540–1546

The *gad* mutation has been identified as a deletion on chromosome 5 within the gene encoding ubiquitin carboxyl-terminal hydrolase L-1 (UCH-L1). The deletion lacks a segment of DNA corresponding to 42 amino acids containing the catalytic site of this protein (Saigoh *et al.* 1999). The role of UCH-L1 renders this mouse a suitable model for investigating neurodegenerative disorders, in which altered function of the ubiquitin system is present.

UCH L-1 is a crucial enzyme for maintaining protein degradation by the proteasome, by generating free monomeric ubiquitin (Osaka *et al.* 2003). Proteasomal dysfunction occurs in neurodegenerative disorders (Chung *et al.* 2001; Davies 2001; Ding and Keller 2001; Halliwell 2002). In Parkinson's disease there is genetic evidence for a contribution of UCH L-1 (Liu *et al.* 2002; Nishikawa *et al.* 2003; Jenner 2003). Our previous proteomic study (Castegna *et al.* 2002a) identified UCH L-1 as one specific target of protein oxidation in Alzheimer's disease (AD) brain, establishing a link between the effect of oxidative stress of brain proteins (Butterfield and Lauderback 2002; Butterfield *et al.* 2001; 2002) and the reported proteasomal dysfunction in AD. However, it is unclear how oxidation affects protein function, owing to the different responses of proteins to oxidation. Analysis of systems in which the oxidized protein displays lowered or null activity might represent an excellent model for investigating the effect of the protein of interest in cellular metabolism and evaluating how the cell responds to the stress caused by its oxidation.

Because of the lack of activity of UCHL-1 in *gad* mouse brain, this animal model was chosen to investigate the effect of dysfunctional UCH-L1 in brain in relation to specifically oxidized proteins. Proteomics appeared to be the most efficient way of performing this study because this method allows screening of both the expression and oxidation of hundreds of proteins at once.

Experimental procedures

Brain samples

Six wild-type and six *gad* mouse brain cortical samples (300 mg) were sonicated for 30 s in 500 μL two-dimensional polyacrylamide gel electrophoresis (2D PAGE) sample buffer (8 M urea, 2 M thiourea, 20 mM dithiothreitol, 0.2% (v/v) Biolytes 3–10, 2% CHAPS and bromophenol blue). Following centrifugation at 14000 *g* for 10 min, the supernatant was collected and the protein concentration was determined by using the RC DC assay (Bio-Rad, Hercules, CA, USA) as described previously (Castegna *et al.* 2002a,b, 2003).

2D PAGE and western blotting

2D PAGE was performed in a Bio-Rad system using 110-mm pH 3–10 immobilized pH gradient (IPG) strips and Criterion 8–16% gels (Bio-Rad). For the first dimension, 300 μg protein was applied to a rehydrated IPG strip, and isoelectric focusing was carried out at 20°C. Before the second-dimension separation, the gel strips were equilibrated for 10 min in 37.5 mM Tris-HCl (pH 8.8) containing 6 M urea, 2% (w/v) sodium dodecyl sulfate, 20% (v/v) glycerol and 0.5% dithiothreitol, and then re-equilibrated for 10 min in the same buffer except that dithiothreitol was replaced with 4.5% iodoacetamide. For detection of protein carbonyls, an index of protein oxidation (Butterfield and Stadtman 1997), Western blots (oxyblots) were obtained. The protein hydrazone was formed by incubating IPG strips with 10 mM 2,4-dinitrophenylhydrazine (DNPH)/1 M HCl for 10 min and 2 M Tris base/30% glycerol for 15 min. A detailed description of the chemistry involved in protein carbonyl formation and analysis has been published (Butterfield and Stadtman 1997). Basically, in the present study protein carbonyls were detected immunochemically by an antibody to the hydrazone formed between protein carbonyls and DNPH, followed by an alkaline phosphate-linked secondary antibody (Castegna *et al.* 2002a,b). The IPG strips were rehydrated as described above and placed on Criterion gels (Bio-Rad). After unstained molecular weight protein standards had been applied, electrophoresis was started. Isoelectric focusing was performed as follows: 300 V for 1 h, then linear gradient to 8000 V for 5 h and finally 20 000 V/h. Second-dimension gels were run at 200 V for 65 min (Butterfield and Castegna 2003). Immunoblotting analysis was performed as described in Castegna *et al.* (2002a).

Sample preparation for matrix-assisted laser desorption ionization-time of flight (MALDI-TOF) mass spectrometry

All mass spectra reported in this study were acquired by the University of Kentucky Mass Spectrometry Facility with an HP 1100 HPLC system modified with a custom splitter to deliver 4 μL/min to a custom C18 capillary column [300 μm (internal diameter) × 15 cm, packed in-house with Macrophere 300 5-μm C18 ; Alltech Associates, Deerfield, IL, USA]. Gradient separations consisted of 2 min isocratic at 95% water : 5% acetonitrile (both phases contain 0.1% formic acid) to begin with; the organic phase was increased to 20% acetonitrile over 8 min, then increased to 90% acetonitrile over 25 min, held at 90% acetonitrile for 8 min, then increased to 95% for 2 min, and finally returned to initial conditions for 10 min (total acquisition time 45 min with a 10-min recycle time). Tandem mass spectrometry (MS/MS) spectra were acquired on a Finnigan LCQ 'Classic' quadrupole ion trap mass spectrometer (Finnigan, Co., San Jose, CA, USA) in a data-dependent manner. Three scans were averaged to generate the data-dependent full scan spectrum. The most intense ion was subjected to tandem mass spectrometry, and five scans were averaged to produce the MS/MS spectrum. Masses subjected to the MS/MS scan were placed on an exclusion list for 2 min.

Tandem spectra used for protein identification from tryptic fragments were searched against the National Center for Biotechnology Information (NCBI) protein databases using a local MASCOT search engine server. Resulting MS/MS spectra assumed the peptides to be mono-isotopic, oxidized at methionine residues and carbamidomethylated at cysteine residues (Castegna *et al.* 2002a,b, 2003). However, a 0.8-Da MS/MS mass tolerance was used for searching. Only the MS/MS data provided identification of proteins, and a typical mass spectrum is represented in Fig. 1.

Probability-based MOWSE scores were estimated by comparison of search results against estimated random match population and were reported as $-10*\mathrm{LOG10}(p)$, where p is the absolute probab-

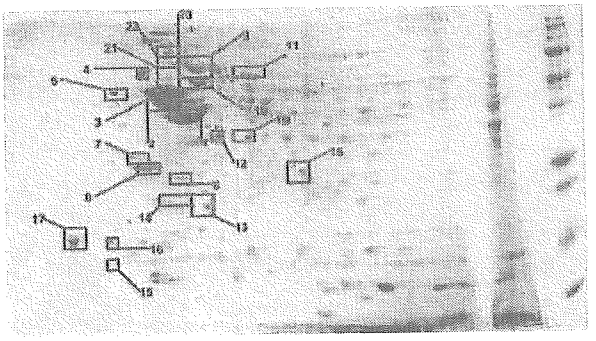

#	Protein
1	β-actin
2	Enolase
3	Tubulin
4	Neurofilament
5	Neurofilament
6	Tyrosine-3-monoyxygenase
7	tyrosine 3/tryptophan 5 -monooxygenase activation protein
8	Rho GDP-dissociation inhibitor 1
9	Heat shock cognate 71 kDa protein
10	neurofilament protein NF-66
11	dihydropyrimidinase related protein-2
12	lactate dehydrogenase 2
13	RIKEN cDNA
14	thioredoxin peroxidase
15	hippocampal cholinergic neurostimulating peptide precursor protein
16	β-synuclein
17	Calmodulin
18	phosphoglycerate mutase
19	malate dehydrogenase
20	Heat shock protein 86
21	dnaK-type molecular chaperone grp78 precursor or 78 kDa glucose-regulated protein precursor (GRP 78)
22	Rab GDP dissociation inhibitor alpha & ATP synthase

Fig. 1 Example of liquid chromatography–MS/MS spectrum. In this case the spectrum is *m/z* 968 from gi/25742763 70-kDa heat-shock protein.

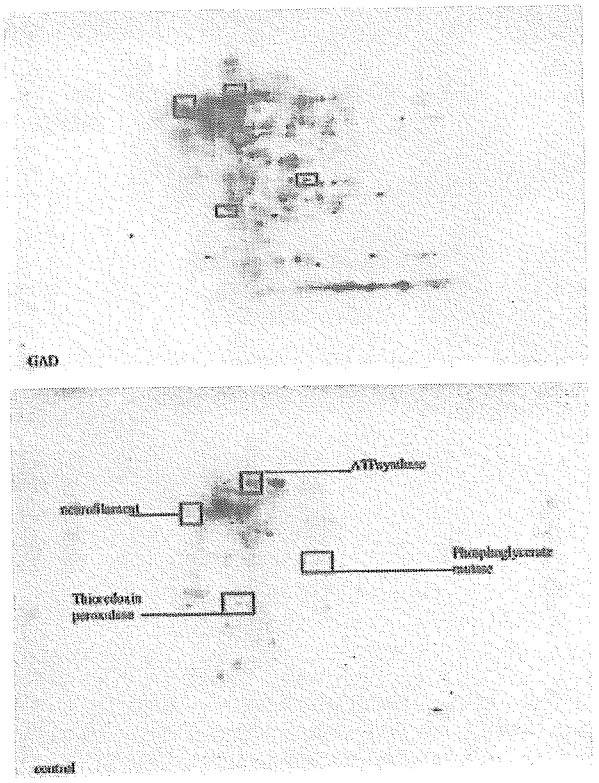

Fig. 2 D gel map of *gad* mouse brain. The proteins corresponding to the 22 spots identified by mass spectrometry are listed. As with most 2D gels, the pH increases from left to right on the abscissa, and molecular mass decreases from top to bottom on the ordinate.

ility. All protein identifications were in the expected size range based on position in the gel.

Statistical analysis

Statistical comparison of carbonyl levels of proteins with anti-dinitrophenyl hydrazone (anti-DNP)-positive spots on 2D oxyblots from *gad* and wild-type, aged-matched control brain samples was by ANOVA. $p < 0.05$ was considered significantly different.

Results

DNPH-positive proteins on the blot were located in the gel map and excised for mass spectrometric analysis as described above. Twenty-two proteins were identified (Fig. 2). Proteins containing reactive carbonyl groups in *gad* and control brain samples were identified by 2D oxyblot analysis (Fig. 3). Comparison of 2D oxyblots with images of Coomassie blue-stained 2D gels from the same samples revealed that many, but not all, individual protein spots in the inferior parietal lobule brain extracts exhibit anti-protein carbonyl immunoreactivity. 2D oxyblots and the subsequent 2D gel images were matched and the anti-DNP immunoreactivity of individual proteins separated by 2D PAGE was normalized to their protein content, obtained by measuring the intensity of colloidal Coomassie blue staining. This procedure allowed comparison of oxidation levels of brain proteins in *gad* and control subjects (Castegna *et al.* 2002a,b; Butterfield and Castegna 2003; Butterfield *et al.* 2003).

Only four proteins exhibited a significant increase in protein carbonyls in *gad* compared with control samples (Table 1). Three of these proteins were identified as phosphoglycerate mutase (1025 ± 187% of control), thioredoxin peroxidase (708 ± 123% of control) and neurofilament L (NF-L) (853 ± 13% of control). ATP synthase was identified together with Rab GDP dissociation inhibitor α; these two proteins have the same isoelectric point (pI) and molecular mass and it was impossible to separate them by 2D PAGE. The oxidation level for this mixture was 154 ± 43% of the wild-type spot. Table 2 presents the unique protein identifier (GI accession number), number of peptides identified, sequences determined, percentage sequence coverage, the probability-based MOWSE score and the *p* value for each oxidized protein identified. Note that the latter is exceedingly small, indicating that the identity established for each protein is correct.

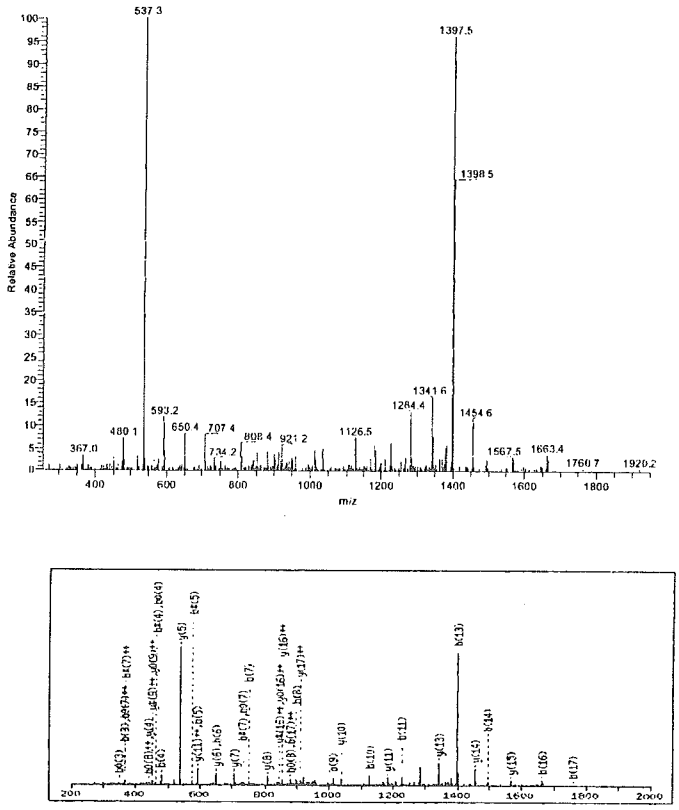

Fig. 3 Oxyblot maps for *gad* (top) and wild-type (bottom) mouse brain proteins, with labeled proteins significantly more oxidized in the *gad* mouse brain samples. The axes are the same as those in Fig. 1.

Discussion

The presence of non-functional UCH L1 in the *gad* mouse results in severe motor neuronal impairment. The results presented here give insight for the first time into the mechanism of neuronal degeneration in the *gad* mouse. Oxidative stress is responsible for NF-L disassembly, which in turn impairs axonal transport, causes demyelination and eventually leads to neuronal atrophy and death.

Table 1 Relative percentage change in specific carbonyl levels in proteomics-identified proteins in *gad* mouse brain compared with wild-type mouse control brain

Identified protein	Specific oxidation (% of control)	p^*
Phosphoglycerate mutase	1025 ± 187	0.05
Thioredoxin peroxidase	708 ± 123	< 0.05
Rab/ATPase (?)	154 ± 43	< 0.04
NF-L	853 ± 13	< 0.04

For each protein, individual anti-DNP immunostain/protein values (obtained from each of six *gad* and six control brains) were averaged and expressed as percentage of control ± SEM. *ANOVA.

Neurofilaments are axonal proteins that participate in the neuronal cytoskeletal structure and play an important role in the process of myelination. NF-L is a target of intensive study in motor neuron disease, in which abnormalities of its assembly, secondary structure and post-translational modifications have been detected (Crow *et al.* 1997; Beckman 1996; Chou *et al.* 1998; Cookson and Shaw 1999; Gelinas *et al.* 2000).

The abnormal accumulation of NF-L in degenerated motor neurons, which is the main pathological feature of amyotrophic lateral sclerosis (ALS), has initiated studies of the relationship between superoxide dismutase 1 mutation, which occurs in familial cases of ALS, and neurofilament accumulation. Superoxide dismutase-initiated nitration of mouse disassembled NF-L showed increases in 3-nitrotyrosine (Crow *et al.* 1997), consistent with the finding that tyrosine is often responsible for stabilization of neurofilament subunits, a stabilization fostered by hydrophobic interactions (Heins *et al.* 1993). Additionally, transgenic mice expressing a point mutation of NF-L exhibit motor impairment (Cote *et al.* 1993).

The hypothesis that neurofilaments might be a target of protein modification in motor neuron diseases is supported by extensive evidence (Beckman 1996; Chou *et al.* 1998; Cookson and Shaw 1999). Other than being targets of protein